FABRICATION AND CHARACTERIZATION OF
Bi-2212 SUPERCONDUCTING
SERAMIC THIN FILMS

2014
M. Sc. Thesis
Electric Electronic Engineering

Esra EVCİN BAYDİLLİ

FABRICATION AND CHARACTERIZATION OF Bi-2212
SUPERCONDUCTING SERAMIC THIN FILMS

A THESIS SUBMITTED TO
THE GRADUATE SCHOOL OF NATURAL AND APPLIED SCIENCES OF
KARABUK UNIVERSITY

BY

Esra EVCİN BAYDİLLİ

IN PARTIAL FULFILLMENT OF THE REQUIREMENTS FOR
THE DEGREE OF MASTER OF SCIENCE IN
DEPARTMENT OF
ELECTRIC ELECTRONIC ENGINEERING

January 2014

I certify that in my opinion the thesis submitted by Esra EVCİN BAYDİLLİ titled "FABRICATION AND CHARACTERIZATION OF Bi-2212 SUPERCONDUCTING CERAMIC THIN FILMS" is fully adequate in scope and in quality as a thesis for the degree of Master of Science.

Assist. Prof. Dr. Mustafa ANUTGAN

Thesis Advisor, Department of Electric-Electronic Engineering

Prof. Dr. İbrahim BELENLİ

Thesis Advisor, Abant Izzet Baysal University

This thesis is accepted by the examining committee with a unanimous vote in the Department of Electric-Electronic Engineering as a master thesis. January 17, 2014

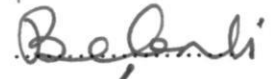| Examining Committee Members (Institutions)	Signature
Chairman : Prof. Dr. İsmail ATILGAN (KBU)	
Member : Prof. Dr. Ahmet VARİLCİ (AIBU)	
Member : Prof. Dr. İbrahim BELENLİ (AIBU)	
Member : Assoc. Prof. Dr. Habibe USLU (KBU)	
Member : Assist. Prof. Dr. Mustafa ANUTGAN (KBU)	

...../ ...... / 2014

The degree of Master of Science by the thesis submitted is approved by the Administrative Board of the Graduate School of Natural and Applied Sciences, Karabuk University.

Prof. Dr. Mustafa BOZ

Head of Graduate School of Natural and Applied Sciences

ii

Esra EVCİN BAYDİLLİ

ABSTRACT

M. Sc. Thesis

FABRICATION AND CHARACTERIZATION OF Bi-2212 SUPERCONDUCTING SERAMIC THIN FILMS

Esra EVCİN BAYDİLLİ

Karabuk University

Graduate School of Natural and Applied Sciences

The Department of Electric Electronic Engineering

Thesis Advisor:

Assist. Prof. Dr. Mustafa ANUTGAN

Prof. Dr İbrahim BELENLİ

January 2014, 58 pages

In this thesis, it was aimed to determine the optimum production parameters in order to obtain Bi-2212 thin films that have high quality electrical and surface morphology properties. DC power, plate temperatures and deposition time parameters were investigated for DC sputtering which was used as the deposition method. Moreover, optimum annealing parameters were determined.

Thin films were produced at 15W DC power and 500 °C plate temperature in both 2 hours and 0.5 hour. Produced films were annealed at different temperatures, after that, they were quenched at 700°C in order to determine the optimum annealing temperature. In addition, annealed films at 860 °C were quenched at different temperatures to investigate the effect of quenching temperature for all films.

Deposited films were used for resistance-temperature measurements at 0.1 mA. Besides, crystal structure and surface morphology were investigated with XRD measurements and SEM images, respectively.

ÖZET

Yüksek Lisans Tezi

Bi-2212 SERAMİK SÜPERİLETKEN İNCE FİLMLERİN ÜRETİMİ VE KARAKTERİZAYONU

Esra EVCİN BAYDİLLİ

Karabük Üniversitesi
Fen Bilimleri Enstitüsü
Elektrik-Elektronik Mühendisliği Anabilim Dalı

Tez Danışmanı:
Yrd. Doç. Dr. Mustafa ANUTGAN
Prof. Dr İbrahim BELENLİ
Ocak 2014, 58 sayfa

Bu tez çalışmasında elektriksel ve yüzey morfolojik özellikleri yüksek Bi-2212 ince film elde etmek için uygun üretim parametrelerinin belirlenmesi amaçlanmıştır. Kaplama yöntemi olarak kullanılan DC püskürtme yöntemi için DC güç, alttaş sıcaklığı ve kaplama süresi parametreleri incelenmiştir. Ayrıca kaplanan filmlerin uygun tavlama parametreleri belirlenmiştir.

Filmler 15W DC güç ve 500 °C alttaş sıcaklığı hem 2 saat hem de 0.5 saat sürede üretilmiştir. Kaplanan filmler farklı sıcaklıklarda tavlanarak, 700 °C'de sıcaklığı dindirilerek uygun tavlama sıcaklığı belirlenmesi hedeflenmiştir. Ayrıca, 860 °C'de tavlanan filmler ise farklı sıcaklıklarda sıcaklığı dindirilerek dindirme sıcaklığının filmler üzerindeki etkisi incelenmiştir.

Kaplanan filmlerin 0,1 mA akım ile direnç-sıcaklık ölçümü yapılmıştır. Ayrıca XRD ölçümleri ile filmlerin kristal yapısı, SEM görüntüleri ile de yüzey morfolojisi incelenmiştir.

Anahtar Kelimeler : Bi-2212, süperiletken ince film, tavlama sıcaklığı.
Bilim Kodu   : 905.1.092

ACKNOWLEDGMENTS

CONTENTS

LIST OF FIGURES

LIST OF TABLES

PART I

INTRODUCTION

All story of superconductivity has started with discovery of liquid Helium (4.2 K) in 1908 by Kamerlingh Onnes. Some scientists such as William Kelvin believed that the electrons pass through the conductor would stop when the temperature of that conductor approaches to absolute zero. In contrast, Onnes and other scientists asserted that resistivity of a conductor could be zero at absolute temperature. Onnes chose mercury for his studies since its purification by distillation is quite good. Onnes observed that the resistance of mercury fell sharply near 4.2 K (-268.8 ^{o}C) and reached immeasurable value (Figure 1.1). Onnes named this new situation 'superconductivity' in which mercury demonstrated zero-resistivity state and so the world became introduced with the concept of superconductivity [1].
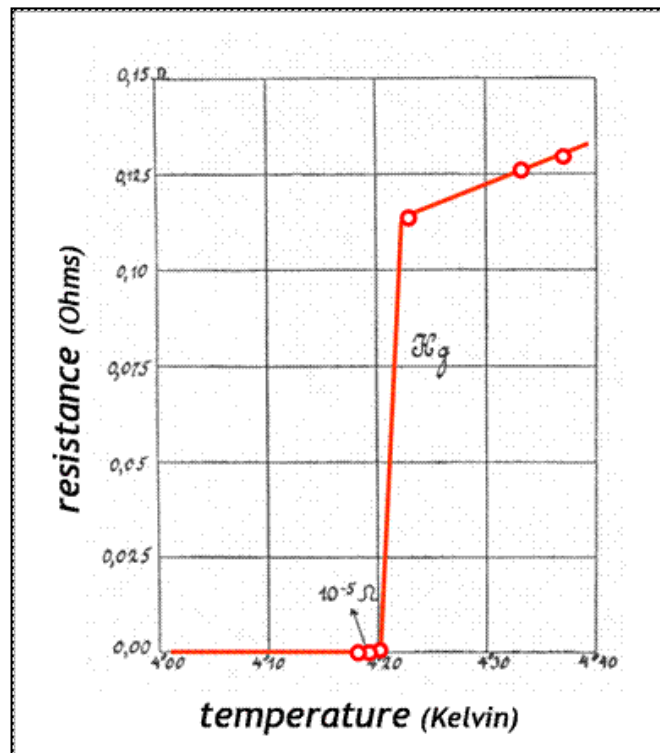
Figure 1.1. Transition of mercury [2].

First part of this thesis includes historical review and literature review. Besides, theoretical background of superconductivity was mentioned. In part II, experimental techniques are described and obtained results were explained. Last part of thesis contains experimental results, reviews and discussions.

1.1. HISTORICAL REVIEW

Idea of superconductivity came up with in 1908, when liquid Helium (4.2 K) was obtained by Dutch physicist Heike Kamerlingh Onnes who investigated the electrical properties of materials at very low temperatures. In 1911, Onnes observed that below 4.2 K, the resistance of mercury decreased to an immeasurable value. Then, Onnes called this phenomenon 'superconductivity' and in 1913, he won the Nobel Prize in Physics for his research in this area [1].

In 1933, Walther Meissner and R. Ochsenfeld discovered another important feature of superconductors, perfect diamagnetism. While they examined the magnetic properties of superconductors, they reached that the conductor, which cooled below its critical temperature, excluded applied magnetic field on it, until transition from superconducting to normal state is completed. This phenomenon known as perfect diamagnetism is also called Meissner Effect [3].

In 1934, F. and H. London suggested the Meissner Effect and predicted penetration depth λ: a characteristic length of penetration of the static magnetic field into a superconductor. Description of the electrodynamics of super-current is known as the London Equations, which explain the resistanceless property of a superconductor and diamagnetism by using classical physics [4]. Ginzburg-Landeau Theory, which is an alternative to the London theory, was executed by V. Ginzburg and L.D. Landau in 1950. Unlike the London theory, Ginzburg-Landeau theory uses quantum mechanics to predict the effect of a magnetic field [5].

Also in 1950, E. Maxwell and C. A. Reynolds explained the inverse proportionality relation between critical temperature (T_c) and isotope mass (M) by using superconducting isotopes of mercury. It is called Isotope Effect [6].

In 1957, according to behaviour of superconductors in an external magnetic field, superconductors are investigated in two types: type-I and type-II, discovered by Alexei Abrikosov [7].

Also in 1957, J. Bardeen, L. Cooper and R. Schrieffer evidenced first widely accepted quantum mechanical theory of superconductors which is called ''BCS'' theory. This microscopic theory explains the physical mechanism of superconductivity [8].

Quantum mechanical tunnelling of Cooper pairs through a thin insulator barrier between two superconductors was proved theoretically by B. D. Josephson in 1962. After a year Josephson's proposal was proved experimentally and today is called Josephson Effect [9].

Until 1970's, because of studies, transition temperatures of newly found superconductors could be raised to only 20 K. In 1973, Nb_3Ge was discovered whose transition temperature is 23 K. This was the highest critical temperature of the metallic superconductors [10].

The year 1986 is the milestone of superconductivity. In IBM Research Laboratory in Zurich, Switzerland, K. A. Muller and J. G. Bednorz synthesized the La-Ba-Cu-O ceramic compound with perovskite structure whose transition temperature is 30K. Thus, the history of high T_c superconductivity started [11]. After discovery of the ceramic superconductors, many scientists studied on synthesis of new compounds by doping different atoms in crystal structure. In February 1987, the research group of K. Wu Ashburn and Paul Chu discovered Y-Ba-Cu-O ceramic compound. They observed that transition temperature reached 93 K, thus, using cheap liquid nitrogen became possible to reach the critical temperature instead of the expensive liquid helium [12].

Also in 1987, Michael et al. introduced a new compound to superconductivity, which is bismuth strontium copper oxide (Bi-Sr-Cu-O) [13].

In early 1988, rise of critical temperature by adding calcium to Bi-Sr-Cu-O system was found by Maeda and his group. This system has three phases depending on the number of the CuO_2 planes: Bi-2201 (T_c=20 K), Bi-2212 (T_c=85 K) and Bi-2223 (T_c=110 K) [14].

In the same year, Tokano and his friends added Lead to the Bi-based compound so the critical temperature reached 110 K [15].

Also in 1988, Sheng and Parkin discovered thallium barium calcium copper oxide (Tl-Ba-Ca-Cu-O) compound, which shows superconducting property and has 125 K critical temperature [16].

In 1992, Oidwaj and his group explored a new stable compound which was obtained by adding Antimony to Bi-based system and transition temperature reached 130 K [17].

In 1993, Hg-based copper oxides $HgBa_2CaCu_3O_{1+x}$ compound, which have the highest T_c value with *133 K*, was explored by Schilling and his group [18]. At 300 GPa, its T_c value reached to 164 K [19].

In 2001, J. Akimitsu et al. discovered superconductive properties of MgB_2 metal alloy. It was attracted more attention due to it has highest transition temperature of 39 K than the other metal alloys [20].

In 2007, Liang and his research group synthesized LaOFeP superconductor by using La-Fe-P alloys and determined its superconductive properties. Its critical temperature is 4.1 K [21].

1.2. LITERATURE REVIEW ON Bİ-2212 THIN FILM

In 1995, Takayuki Ishibashi and his group studied on growth of $Bi_2Sr_2Ca_{n-1}Cu_nO_{2(n+2)+\delta}$ (n=2,3) thin film on $SrTiO_3$ (001) by molecular beam epitaxial with growth interruption method due to the advantage of its enhanced surface diffusion of

atoms. They determined that growth interruption technique enhanced the 2D growth and suppressed the precipitation of impurities. Besides, they verified by reflection high-energy electron diffraction (RHEED) observations that the deposited atoms with coverage less than half a unit layer were effectively crystallized under a sufficient time of growth interruption [22].

In 1996, Koichi Mizuno and Kentaro Setsune produced $Bi_2Sr_2Ca_{n-1}Cu_nO_{2(n+2)+\delta}$ (n=1,2) on $SrTiO_3$ and MgO substrates at 650 °C substrate temperature in their study. The onset critical temperature of produced films were about 80 K and offset temperature were around 60 K. In this study crystallinity quality of this Bi-based oxide thin films were investigated. According to crystalline measurements of thin films (RHEED, Rutherford backscattering spectroscopy (RBS) and X-ray diffraction XRD measurements), they determined $SrTiO_3$ substrates are better than MgO substrates at obtaining Bi-based oxides with good crystallinity. The principal reason might be the lattice-matching conditions. They also elucidated that the crystallinity of BSCCO films has been improved by introducing a BSCO buffer layer and these results suggested that lattice matching is the most important factor for Bi-based oxide films with good crystallinity [23].

In 1996 again, J. Wiesner and his friends irradiated produced Bi-2212 thin films with 200 MeV ^{40}Ca, 1162 MeV and 2640 MeV ^{197}Au and 1404 MeV ^{238}U ions and investigated the radiation induced defects in the films with high resolution electron microscopy (HREM). According to these examinations, they said that swift heavy ions produce well-defined latent columnar tracks consisting of totally amorphized material divided by a sharp transition from the surrounding crystalline material and continuous columnar defects (^{197}Au, ^{238}U) are more efficient pinning centres than scattered defect cascades (^{40}Ca) [24].

In 1997, E. Brecht and his group studied on Bi-2212 thin film on (110) $SrTiO_3$ substrates by inverted cylindrical magnetron sputtering. They obtained two competing growth orientations, which are inclined domains and perpendicular domains by structural analysis [25]. In the same year, J. Dreben et al. prepared BiSrCaCuO thin films and vertical S-N-S (2212/2201/2212) junctions on SrTiO and

LaAIO substrates. Obtained film was 40 nm thick and had 84 K T_c value. According to structural analysis, they decided that the film substrate interface in the films was considerably sharper and had a better planarity, if the layer-by-layer MBE process started with a Sr-O layer instead of a Bi-O layer [26].

In addition, in this year, A. Pfuch and his group examined the properties of bi-crystalline and bi-epitaxial BSCCO-2212 Josephson junctions prepared on SrTiO substrates. Prepared direct current superconducting quantum interference devices (DC SQUIDS) worked up to about 75 K by using these junctions. They purposed show the influence of external magnetic field and microwave radiation on the intrinsic Josephson junction behaviour [27]. Moreover, in 1997, P. Haibach and his group fabricated $Bi_2Sr_2CaCu_2O_{8+\delta}$ by DC-Magnetron sputtering on vicinal (110) SrTi03 substrates. According to anisotropic transport measurements, they determined that the superconducting transition temperature is approximately 47 K and the normal state resistivity along two perpendicular paths differ by a factor of 13.5 [28].

In 1998, E. Brecht et al. deposited Bi-2212 thin film on (110) $SrTiO_3$ and they obtained two competing growth orientations which were c-axis oriented perpendicular to the substrate surface and domains inclined with the c-axis almost parallel to [100] and [010] substrate directions. They showed that the first growth layer at the interface of the c-axis oriented grains is the Bi–O layer by HREM investigations [29].

In 2001, R. Rössler et al. prepared $Bi_2Sr_2Ca_{n-1}Cu_nO_{2(n+2)+\delta}$ (n=1,2,3) thin film on (001) $SrTiO_3$ substrates by pulsed laser deposition technique to optimize the substrate temperature, laser fluence and post-annealing conditions. They declared that the surface morphology, texture, crystallinity and stoichiometry of $Bi_2Sr_2CaCu_2O_{8+\delta}$ (Bi-2212) thin films strongly depend on the fabrication parameters. They produced c-axis oriented Bi-2212 thin films that J_c is $2x10^{-6}$ A/cm^2 and T_c=82 K [30].

In 2001 also, Shunichi Arisawa et al. investigated the growth mechanism of Bi-2212 ribbon like thin films that were analyzed by Auger electron spectroscopy. From the

results of AES analyses and high temperature optical microscopy, thin liquid phase growth mechanism was suggested. In addition, they found that there were some precipitates other than Bi-2212 phase [31].

In 2002, Sang Sub Kim et al. analyzed effects of oxygen ion irradiation followed by thermal annealing of single phase Bi-2212 thin films on SrTiO (001) synthesized by pulsed laser deposition were studied. They observed ion irradiated and thermally annealed ones show leaf-like grain morphology and a significantly improved electric resistivity behaviour unlikely as-deposited film. They claimed that amorphization by ion irradiation followed by re-crystallization by thermal annealing, may be a new method to enhance superconducting properties of Bi-2212 films [32]. Again, in 2002, Tetsuji Uchiyama et al. studied on hetero-epitaxial growth and transport properties of Josephson junctions of the 3 layer films which were made of YBCO/Bi-2212/YBCO. According to X-ray diffraction, results produced from each layer showed good hetero-epitaxial growth. They found that the transport properties of the mesa junctions depend on the ex situ annealing conditions, which is important for obtaining superconductivity after fabricating the mesa structures [33].

In 2002, Yanjing Su and his friends examined the growth of ribbon-like thin film on a flat Ag (001) film by applying atomization method. They produced extremely thin Bi-2212 ribbon-like thin films with well-defined composition and high c-axis orientations on flat Ag (001) thin film substrates were grown. They suggested that a liquid phase wetting mechanism by their in situ HTM (High Temperature Microscope) observation for the formation mechanism of ribbon-like thin films [34]. Moreover, in 2002, K. Endo et al. reported on the successful preparation of intrinsic Josephson junctions on high-quality BSCCO thin films grown by MOCVD. Produced mesas were effectively structured on the grown films by the liquid-nitrogen-cooled dry etching method. They observed that typical I–V characteristic in the c-axis direction of a BSCCO film showed the hysteresis and multiple resistive branches [35].

In addition, in 2002, Satoru Kaneko and his group achieved epitaxial growth of $Bi_2Sr_2Ca_1Cu_2O_X$ (Bi-2212) substrate using the fourth harmonics of YAG pulsed

laser. They determined that by adjusting the beam incidence angle, epitaxial growth was verified for Bi-2212 deposited at the repetition rate of 2 Hz [36].

In 2004, E. Kume, H. Fujino, X. Zhao and S. Sakai prepared Bi-2212 thin films by a pulse laser deposition (PLD) method followed by post-annealing. The thin films, which were about 200 nm, were grown on MgO substrates at 400–630 °C. Post-annealing were performed at 860–880°C in a tubular furnace with mixed gas (Ar: O 2 ¼ 93:7, 1 atm, 0.2 l/min flow) for 3 h. They observed that Bi content did not decrease with the increase of post-annealing temperature up to 870°C and the critical temperature of film was 78 K [37]. In 2004 again, H. Salamati and P. Kameli prepared a series of Bi-2223 samples with different fractions of Bi-2212 phase and investigated its effect on the inter-granular properties. They found that the Bi-2212 phase exists within the grain boundaries and plays a role of weak links and consequently reduces the inter-granular coupling [38].

In 2005, H. El. Alami et al. studied on growth, electrical and structural properties of Bi-2212 thin films which were produced by MBE technique. They observed that discontinuities in the $(BiO)_2$ bilayers but this ''nano-structuration'' does not increase the value of T_c. Moreover, they determined that the 2D character of the conductivity was affected by the segregation of CuO blocks by a model of percolation [39].

In 2008, Zon Mori et al. investigated growth conditions of 2212 thin films by DC magnetron sputtering. They obtained that J_c (critical current density) of the thin films was 1×10^{-5} A/cm^2 and T_c was 80K [40].

In 2009, S. Watanabe and friends analyzed the characteristics of in-plane orientation for c-axis oriented Bi-2212/MgO thin films fabricated by MOD with a 2-step heat treatment. They declared that the in-plane orientation in the initial stage depended on the precursor-fabrication temperature [41].

In 2010, K. Hamanaka, T. Tachiki and T. Uchida fabricated Bi-2212/MgO thin films with thicknesses of 40–240 nm by MOD using the optimized firing conditions. They obtained good uniformities in the in plane orientation and surface morphology for the

films of 120 and 240 nm. They determined that the resistivity at the on-set T_c decreased and J_c along the a–b plane at 4.2 K increased with increasing the film thickness. The maximum J_c obtained for the films of 240 nm was 1.1×10^{-6} A/cm^2 at 4.2 K [42]. Moreover, in this year, Jeffrey C. De Vero and his group grew Bi-2212 thin film on MgO (100) using 1064 nm infrared-pulsed laser deposition with post heat treatment. Smooth, homogeneous and highly c-axis oriented films were obtained after heat treatment. They announced that the morphology could be controlled through heat treatment steps after deposition [43].

In 2011, Xiaoming Yu and his friends used sol-gel-spin-coating method to grow $Bi_2Sr_2CaCu_2O_{8+\delta}$ thin film on (100) $SrTiO_3$ substrates. They obtained single phased films that T_c onset value is 97.7 K [44].

In the same year, Jeffrey C. De Vero et al. studied on Y-doped Bi-2212 thin films on MgO (100) substrates by infrared-pulsed laser deposition (IR-PLD). They observed that the average compositions of the films have the same stoichiometry as the target and the electrical properties of the grown Y-doped Bi-2212 films exhibit the expected electrical properties of the bulk Y-doped Bi-2212 which is attributed to the stoichiometry transfer of material by IR-PLD [45].

In 2013, O. Nane et al. investigated the effects of post-annealing temperature on Bi-2212 thin films on MgO PLD. Obtained film had 82 K T_c value and 3×10^{-7} A/cm^2 J_c value. They determined that optimum annealing temperature was 860 °C [46].

1.3. THEORITICAL BACKGROUND

1.3.1. Zero Resistivity

A basic feature of superconductivity is the conduction of the electric current without any resistance. When a current pass through an ordinary conductor, because of the vibrations of lattice atoms, electrons collide with these atoms and are scattered. Owing to these collisions, momentum of electrons alters and electrons transform

their mechanical energy to heat. In this way, a resistance against conduction is occurred [47].
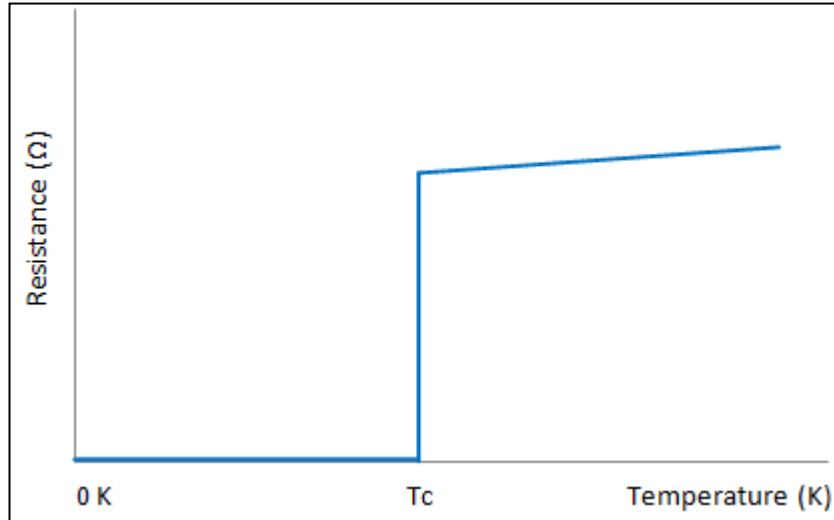
Figure 1.2. Resistance versus temperature graph of a superconductor [48].

In case of superconductivity, lattice structure becomes more regular by means of that the atomic vibrations become negligible and electron couples, which are known as Cooper pairs, carry the current. The bonds between these couples are so strong and even if they are far away from each other, collision energies of the lattice atoms are not sufficient alone, so, they go out of the lattice before interacting with atoms [49]. Thus, electrons can move without losing energy and conductor resistance is eliminated in superconductor state as can be seen in Figure 1.2. Superconductive state occurs below a certain temperature, which is called critical temperature, or transition temperature (T_c).

1.3.1.1. Critical Temperature (T_c)

The temperature at which the resistance disappears or material passes from normal state to superconductive state is called critical temperature or transition temperature, illustrated by T_c. Every superconductor has specific critical temperature. These temperature values for some metals, alloys and HT_c superconductors can be seen in Table 1.1.

Table 1.1. The T_c values of some metals, alloys and HT_c superconductors [10,12,14,16,19,20,50].

Metals	T_c (K)	Alloys	T_c (K)	HT_c	T_c (K)
Sn	3.7	MgB_2	39	LSCO	38
In	3.4	Nb_3Sn	18	Y-123	93
Cd	0.56	Nb_3Ge	23	Bi-2212	85
Pb	7.2	Pb-Bi	8	Bi-2223	110
Al	1.1	Ta-Nb	6.3	Tl-1224	125
Tl	2.4	LaOFeAs	26	Hg-1223	133
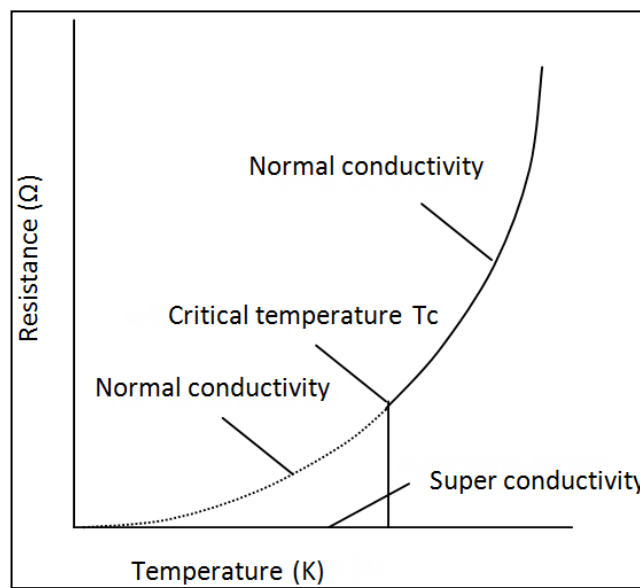
Figure 1.3. Change in resistance with temperature of a superconductor and normal conductor [51].

As shown in Figure 1.3, when the temperature of the material drops below T_c, electrical resistance disappears. On the other hand, when the temperature of the material is above T_c, the material demonstrates regular metallic properties.

1.3.2. The Meissner Effect

In 1933, Walther Meissner and R. Ochsenfeld researched magnetic properties of superconductors and discovered a basic feature of the superconductivity, which is called Meissner Effect [3].

When a magnetic field is applied on a superconductor material, which is cooled until critical temperature in a magnetic field, because of the Lenz Law, a magnetic flux occurs in section that is close to the surface of the material. Because of this flux, a magnetic field is induced in the material surface. This field is in the opposite direction of the external applied field and prevents entrance of the external field into the material [52]. The exclusion of magnetic field from material is shown in Figure 1.4.
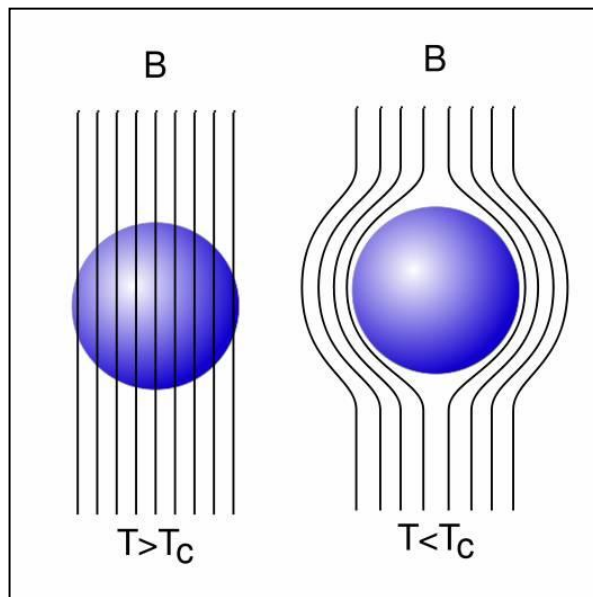
Figure 1.4. Magnetic behaviour of a superconductor [53].

In Figure 1.5 a), there is a normal situation with a ceramic disc magnet. As it is seen, magnetic field lines originate at the North Pole and end at the South Pole. In Figure 1.5 b), the magnet is locating on the surface of superconducting material above its critical temperature. As shown in figure, the magnetic field lines penetrate paramagnetic surface and return into the South Pole. Figure 1.5 c), shows that when a magnet, which is locating on the superconducting material at its critical temperature, the magnetic field lines can no longer penetrate the surface, which is now diamagnetic. As it is seen in Figure 1.5 d), due to inability of the magnetic field lines to enter the South Pole when the magnet is in contact with the superconductor, the rule of magnetic field lines to end at the South Pole is obeyed only if the magnet levitates the superconductor.
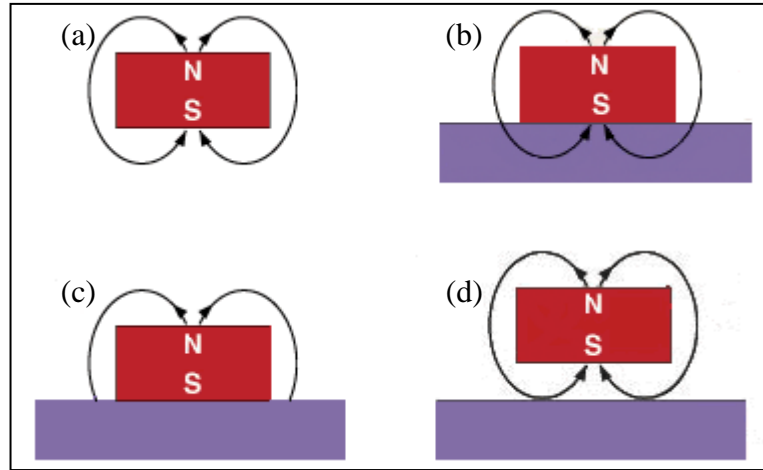
Figure 1.5. Illustration of Meissner effect mechanism. a) a ceramic disc magnet, b) the magnet and superconducting material at T>Tc, c)T=Tc, d) T<T$_c$ [54].

1.3.2.1. Critical Magnetic Field

One of the most basic parameters of superconductivity is the critical magnetic field. While the sample is in its superconductive state and applied magnetic field is raised slowly, magnetic field penetrates into the sample at a certain point. Hence, superconducting state is disappeared. This is called as critical magnetic field and illustrated by H$_c$ [52].

The temperature dependence of the critical magnetic field of a superconductor is given as:

$$H_c = H_0 \left[1 - \left(\frac{T}{T_c} \right)^2 \right]$$
(1.1)

Here, H$_0$ is the critical magnetic field at absolute zero temperature. This limit depends on the superconductor material and temperature. Critical magnetic field values of some superconducting materials can be seen in Table 1.2.

Table 1.2. Critical field values of materials [55, 56].

Material	Critical Field (T)	Material	Critical Field (T)
NbTi	15	YBa_2CuO_7	150
Nb_3Sn	24.5	$Bi_2Sr_2Ca_2Cu_3O_{10}$	250
Nb_3Ge	38	$TlBa_2Ca_2Cu_3O_9$	100
MgB_2	30	$HgBa_2Ca_2Cu_3O_8$	150

1.3.3. Type I and Type II Superconductors

According to magnetic behaviours against applied field, superconducting materials are investigated in two groups; type I and type II. While generally pure metals show type I superconducting properties, alloys and transition metals show type II superconducting features [57]. Although mechanism of superconductivity of type I and type II superconductors is same, Meissner effect operates completely different for these two types of superconductors [52].
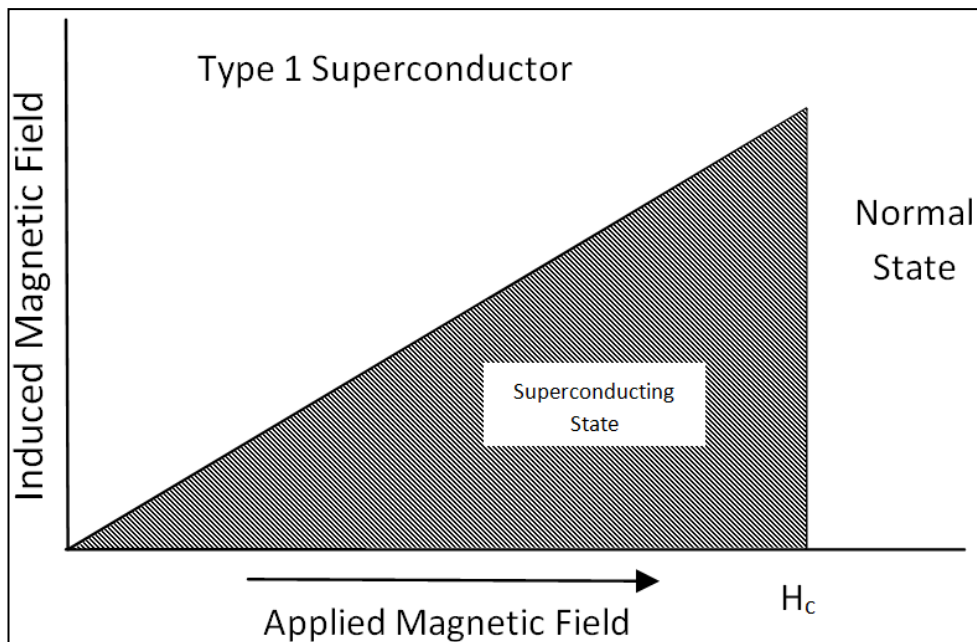
Figure 1.6. Behaviour of Type I superconductors in an applied magnetic field [58].

Graph of magnetic field of a type I superconductor versus applied magnetic field is shown in Figure 1.6. An external magnetic field (horizontal coordinate) is applied to a type I superconductor in induced magnetic field (vertical ordinate) quite void that

14

applied field in as much as there is a sudden change from the superconducting state to a normal state [59].

Figure 1.7 is the graph of induced magnetic field of a type II superconductor versus applied magnetic field. As can be seen in Figure, Type II superconductor is in an increasing magnetic field. Different from type I, this graph has Hc_1 and Hc_2 values. The superconductor excludes all magnetic field lines below Hc_1 value. Between Hc_1 and Hc_2, the field begins to penetrate into the material. In this case, material is in mixed state, which means some of the material in the normal state and other part still superconducting state. Above Hc_2 value material is in normal state [59].
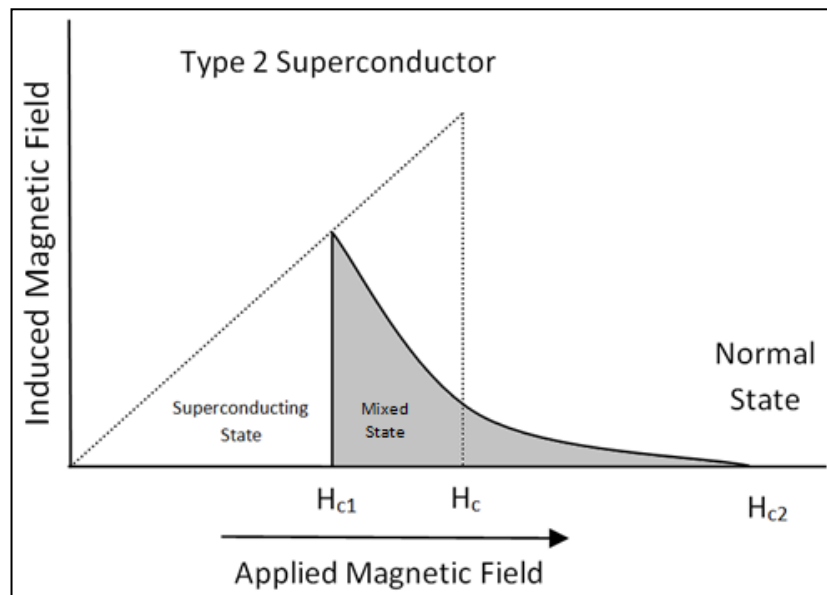
Figure 1.7. The behaviour of Type II superconductor in an applied magnetic field [60].

Since the normal superconductor transition of the first type superconductors is very sharp and the values of H_c are very low, type I superconductors are not preferred to produce superconducting magnets. Nevertheless, second type superconductors have high upper critical magnetic field value and can carry high current, therefore type II superconductors are used for production of superconductor magnets.

1.3.3.1. Critical Current Density

The value of the maximum current carried by the superconductor material is called critical current density, which is denoted by J_c [52]. Critical current density is one of the important parameters like critical temperature and critical magnetic field. As shown in Figure 1.8 the critical surface for a Type II superconductor is the boundary between superconductivity and normal resistivity in three-dimensional diagram. The applied field (B), the temperature (T) and the current density (J) must be maintained below the critical surface in order to retain superconductivity [61].
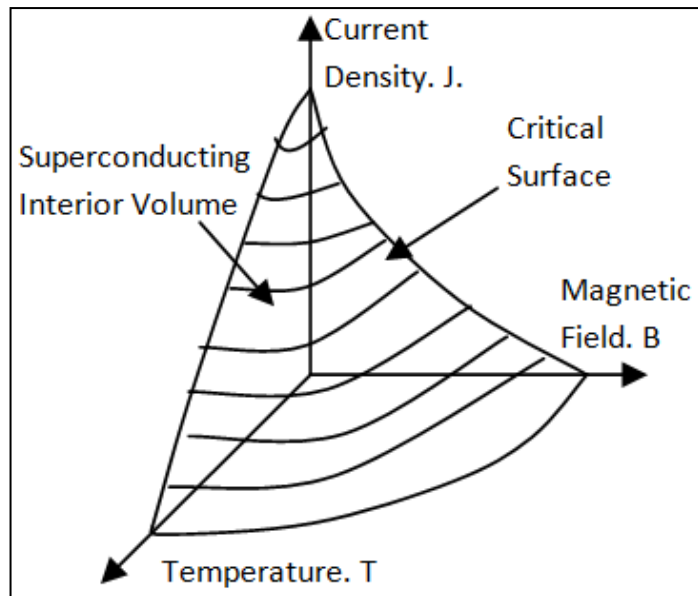
Figure 1.8. Plotted in 3 axes form of a critical surface and the maximum values of temperature, electrical current and magnetic field are interdependent [61].

In a superconducting material, transition to the normal state not only occurs by excess of critical temperature and critical magnetic field but also excess of critical current value. If the current flowing through the material exceeds the critical value, resistance will increase. Critical current density is calculated by Eq. 1.2.

$$J_c = \frac{I_c}{S} \qquad (1.2)$$

Where I_c is critical current value, S is the cross-sectional area of the material [52].

1.3.4. BCS Theory

Until 1957, proposed theories tried to explain the behaviour of superconductive materials mathematically. Although penetration depth and coherence length were added to the literature by London Equations and Ginzburg-Landau Theory respectively, they did not serve the account how superconductivity mechanism works. In 1957, John Bardeen, Leon Cooper and John Schrieffer brought a microscopic initiative, and a precise definition of superconductivity was made [8]. They took account from constructive interaction between electrons and lattice.
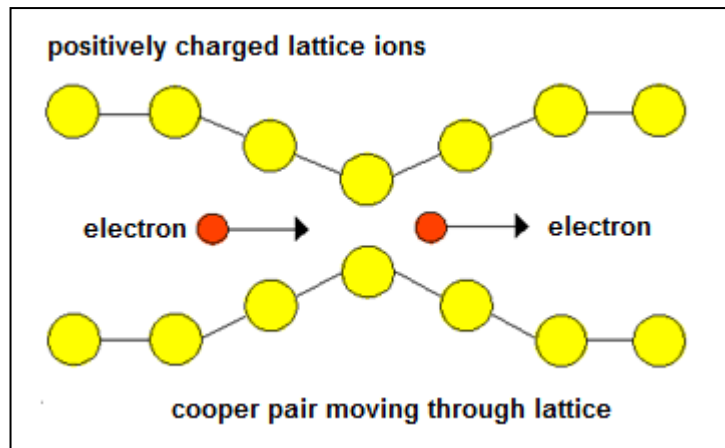
Figure 1.9. Cooper pair moving through lattice [62].

Cooper explained that atomic lattice vibrations were directly responsible for composition of the entire current. They enforce the electrons to pair, which pass all of the obstructions that cause the resistance in conductor. These pairs are called cooper pairs. As it is known that, normally, electrons repel one another. However, this is opposite for superconductors because of phonons. Packets of sound waves are found in the lattice as it vibrates. According to BCS Theory, when a negatively charged electron passes by positively charged ions in the lattice is distorted. Thus, emitted phonons form the flute of positive charges around the electron. Figure 1.9 shows the distorted lattice wave because of attraction due to moving electron. Firstly, an electron passes and lattice returns to its normal position. Then a second electron is taken into the flute. Owing to this process, these two electrons attract one another and now, they are cooper pairs. Due to forces that are performed by phonons, natural

17

repulsion of electrons disappears. When cooper pairs pass through the conductor, they are coherent. Phonons eliminate the repulsion between electrons that are separated by some distance. The attraction between the negative electron and positive ion causes a vibration until the other cooper pair absorbs the vibrations. In this way, the electron emits a phonon then other electron absorbs the phonon. This exchange provides the cooper pairs together. Figure 1.9 also shows that two electrons are called cooper pairs [59, 63].

1.3.5. High T_c Superconductors

All superconductors, which do not contain Cu-O plane, were discovered before the year 1986 that are named low T_c superconductors. Today, nearly regardless of the T_c value, superconductors that have layered structures, which have Cu-O plane, are called High T_c Superconductors (HT$_c$). At the beginning from 1986, La-Ba-Cu-O, Y-Ba-Cu-O, Bi-Sr-Ca-Cu-O, Tl-Ba-Ca-C-O and Hg-Ba-Ca-Cu-O were found and Hg-Ba-Ca-Cu-O system has highest ever T_c value with 164 K. A direct proportion between the number of copper oxide layers and the critical temperature can be supposed in these compounds.

Because the coherence length is quite smaller than the penetration depth, almost all HT$_c$ superconductors are Type II superconductors [7].

Most important property of HT$_c$ superconductors is having critical temperature above the liquid Nitrogen (77 K), which is very easy and cheap to obtain. The major difference between High T_c Superconductors and Low T_c superconductors is that HT$_c$ superconductors are non-homogeneous. Since HT$_c$ superconductors have the granular or ceramic structure, they are brittle [64].

HT$_c$ superconductors are easily affected even by the humidity in the air. In addition, they are mechanically vulnerable because of the temperature fluctuations at low temperatures. These are the main disadvantages of High T_c superconductors.

1.3.5.1. BSCCO System
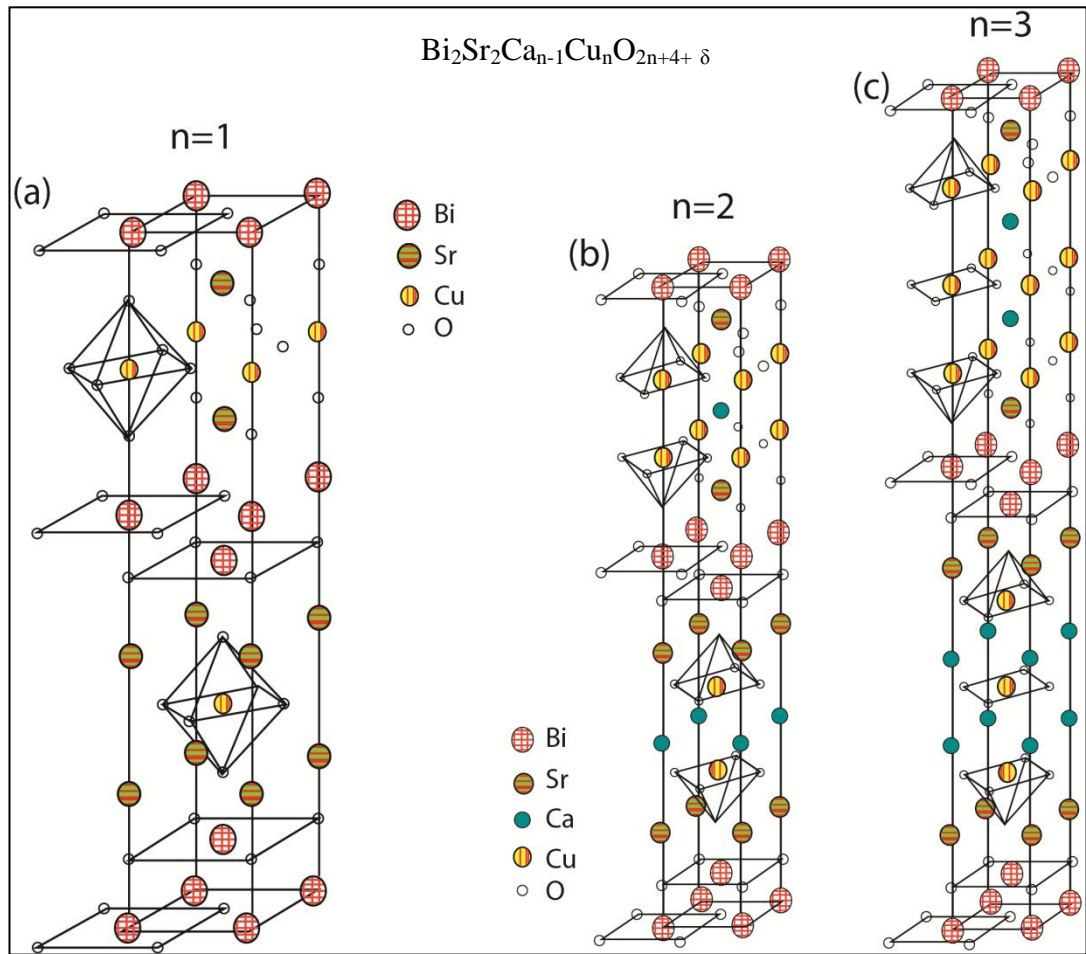
Figure 1.10. Perovskite structures of BSCCO family. Crystal structure is a) Bi-2201, b) Bi-2212 and c) Bi-2223 [65].

Bi-based system is attractive since it is not poisonous and it does not contain rare elements; hence, it is widely used for various applications and fundamental research. BSCCO family according to general formula of $Bi_2Sr_2Ca_{n-1}Cu_nO_{2n+4+\delta}$ and depending on number of Cu-O planes (n), has three different phases which are n=1 (2201), n=2 (2212) and n=3 (2223) [66]. Each of them has different crystal structures and T_c increases with increasing n value.

BiSrCuO superconducting system is found by Michael et al. in 1987 [13]. Afterwards, Maeda and his group discovered BiSrCaCuO by adding Ca and transition temperature increased from 22 K to 85 K [14].

Bi-based system is attractive since it is not poisonous and it does not contain rare elements; hence, it is widely used for various applications and fundamental research. BSCCO family according to general formula of $Bi_2Sr_2Ca_{n-1}Cu_nO_{2n+4+\delta}$ and depending on number of Cu-O planes (n), has three different phases which are n=1 (2201), n=2 (2212) and n=3 (2223) [66]. Each of them has different crystal structures and T_c increases with increasing n value.

$Bi_2Sr_2CuO_6$ Phase

Low T_c phase, n=1, has 20K T_c. As can be seen in Figure 1.10 a), Bi-2201 phase consist of layered structure of BiO/SrO/CuO/SrO/BiO and system has a tetragonal structure. Lattice parameters of system are a = b = 5.39 Å, c = 24.4 Å [66]. In this phase, Cu atoms are surrounded by six O atoms. Oxygen composes octahedral of CuO_6 that is extremely long. The bond lengths and the number of oxygen atoms of Bi-2201 are given in Table 1.3.

Table 1.3. Composed bonds, length of bonds and oxygen content of Bi-2201 [67].

Bond	Bond Length (Å)	# of Oxygen Atoms
Cu-O (1)	1.90	4
Cu-O (2)	2.58	2
Bi-O (2)	2.00	1
Bi-O (3)	2.20	1
Sr-O (1)	2.53	2
Sr-O (2)	2.95	1
Sr-O (3)	2.87	1

$Bi_2Sr_2CaCu_2O_8$ Phase

Crystal structure of $Bi_2Sr_2CaCu_2O_8$ phase or namely Bi-2212, which has the 85 K critical temperature value, is very similar to Bi-2201 phase. The difference of these two structure is Bi-2212 is arranged like BiO/SrO/CuO/Ca/CuO/SrO/BiO by adding Ca between CuO planes. As it seen Figure 1.10 b), system is shaped CuO_5 pyramids and Cu is surrounded by five oxygen atoms that are located at the corners of the square pyramid. Depending on the applied annealing process unit cell can be

20

orthorhombic or tetragonal. Unit cell parameters of orthorhombic structure are a=5.39 Å, b=5.41 Å and c=30.8 Å; those of tetragonal system are a=b=5.40 Å, c=30.60 Å [66]. Bond lengths and the number of oxygen atoms for the Bi-2212 phase are given in Table 1.4.

Table 1.4. Composed bonds, length of bonds and oxygen content of Bi-2212 [67].

Bond	Bond Length (Å)	# of Oxygen Atoms
Ca-O (1)	2.52	8
Cu-O (1)	1.91	4
Cu-O (2)	2.16	1
Bi-O (2)	2.22	1
Bi-O (3)	2.71	4
Sr-O (1)	2.56	4
Sr-O (2)	2.74	4
SrO (3)	2.91	1

$Bi_2Sr_2Ca_2Cu_3O$ Phase

In BSCCO, family Bi-2223 phase has the highest critical temperature value of 110K and is composed of the layers of BiO/SrO/CuO/CaO/CuO/CaO/CuO/SrO/BiO. Shown in Figure 1.10 c), atoms of CO_2 are surrounded by four oxygen atoms. Structure has the tetragonal unit cell and the lattice parameters are a=b=5.4 Å, c=37.1 Å [66]. Bond lengths and the number of oxygen atoms for the Bi-2223 phase are given in Table 1.5.

Table 1.5. Composed bonds, length of bonds and oxygen content of Bi-2223 [67].

Bond	Bond Length (Å)	# of Oxygen Atoms
Ca-O (1)	2.48	8
Cu (1)-O (1)	1.91	4
Cu (1)-O (2)	2.31	1
Cu (2)-O (1)	1.91	4
Sr-O (2)	2.65	4
SrO (3)	2.77	4
BiO (2)	2.99	1
BiO (3)	2.03	1

1.3.6. Substrate Selection

Julia M. Phillips claimed the importance of substrate selection as follows [68]:

"One of the important parameters of production of thin film is the substrate selection. Ideally, the substrate should provide only mechanical support but not interact with the film except for sufficient adhesion. In practice, the substrate exerts considerable influence on film characteristics. The importance of substrate selection in dictating all aspects of film growth from ease or even feasibility of growth to film quality cannot be overemphasized. A number of issues are critical in substrate selection for thin film growth, regardless of the details of the film to be produced."

Mismatch between substrate and film is very effective on critical temperature value. Small mismatch value provides high critical temperature value and smooth film surface. Lattice mismatch is calculated by the formula;

$$2(a_s - a_f)/(a_s + a_f) \hspace{3cm} (1.3)$$

where a_s and a_f are the lattice parameters of the substrate and the film, respectively. Table 1.6 gives mismatch values of some substrates and $Bi_2Sr_2CaCu_2O_8$ in which lattice constant is 3.815 Å.

Table 1.6. Lattice parameters and lattice mismatch values for various substrates [69].

Substrate	a_s (Å)	Mismatch (%)
(100) MgO	4.213	+9.86
(100) SrTiO$_3$	3.904	+2.31
(001) NdGaO$_3$	3.861	+1.20
(001) LaSrGaO$_4$	3.843	+..47
(001) LaAlO$_3$	3.788	-0.72
(001)YAlO$_3$	3.716	-2.65

1.3.7. High T$_c$ Superconductive Thin Film Deposition

HTS (Hihg Temperature Superconductor) thin films have an important role in explanation of HTS principle mechanism. Besides, HTS thin films can be applied on various applications such as bolometers and SQUIDs [42]. On the other hand, all

HTc (High Critical Temperature) compounds consist of least 4 elements, which are highly reactive, complicate the optimization of thin film production parameter. All HTS materials include oxygen that acts for the determination of the various properties of films like grain boundaries. Electrical and superconductive properties of films are quite sensitive to anisotropy in materials. All these features effect adversely the reproducibility of structural properties of thin films and make it difficult.

1.3.7.1. Thin Film Deposition Techniques

Many thin film fabrication processes have been developed to produce high quality and repeatable thin films. These techniques are divided into two main headings: physical vapour deposition (PVD) and chemical vapour deposition (CVD). Sputtering, Pulsed Laser Deposition (PLD) and Molecular Beam Epitaxy (MBE) are the most commonly used PVD methods. Metal Organic Chemical Vapour Deposition (MOCVD) is widely used CVD process [45].

1.3.7.2. Sputter Deposition Method

Sputter is one of the most commonly used physical vapour deposition process. Sputtering, which is discovered in 1852 alternative to thermal evaporation, is firstly used for production of thin film by Langmuir in 1920 [70]. When a solid surface (target) is bombarded by energetic charged particles such as accelerated ions, due to collision of surface atoms and energetic charged particles, back scattering occurs in target. This condition is called sputtering. Owing to the collision of scattered surface atoms and energetic charged ions, sputtering the deposition of atoms scattered from a nearby surface. Sputtering occurs by plasma, which is accelerating by charged particles in surface. Plasma is partially ionized gas of large atomic mass [71–73].

As shown in Figure 1.11 two parallel plates, which are connected to a power supply, are placed in a vacuum system. In such a DC discharge process, if voltage is high enough, the field in reactor achieve a breakdown in gas, so, between two electrodes, a high voltage arc winks. This arc causes formation of a large amount of ions and free electrons. Due to electric field in process chamber, electrons are accelerated

towards positively charged anode; ions are accelerated toward negatively charged cathode. Ions move across the tube and collide with cathode. Thus, a second electron becomes free and accelerated towards anode, again. When voltage is high enough and high-energized electrons collide with neutral atoms in-elastically, much more ions are occurred. Therefore, secondary electrons are free and formation of ions keeps plasma on [74].
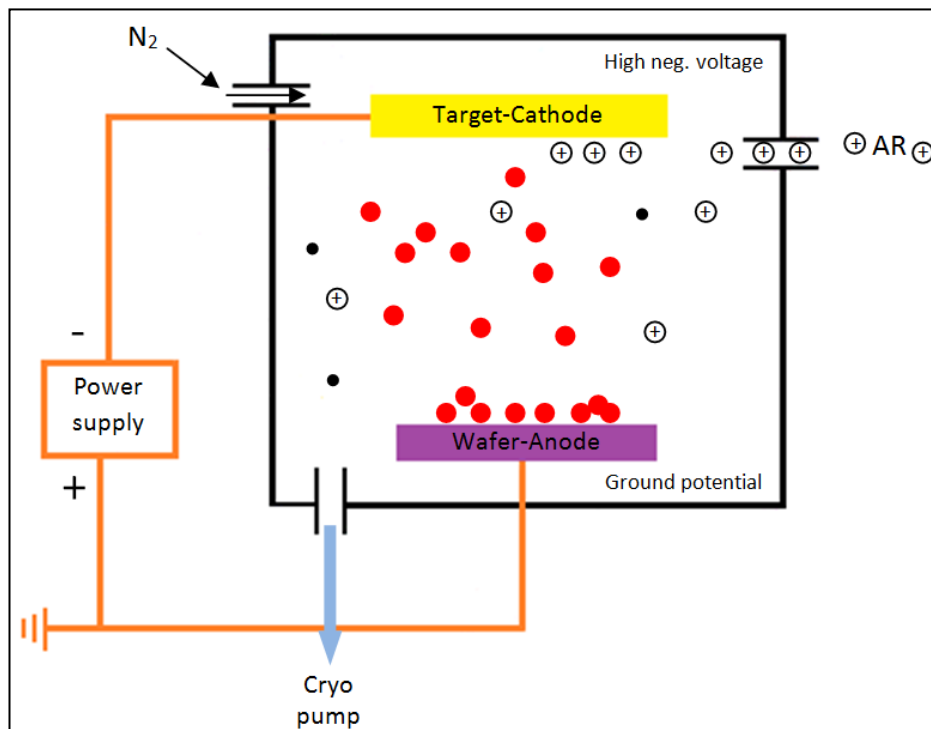
Figure 1.11. A simple diagram of a plasma reactor [75].

Displacement ratio of surface atoms due to ion bombardment is called sputter yield (Y), which is the number of incident ions per emitted particle from the target; it is calculated by;

$$Y = (\text{\# of emitted particle}) / (\text{\# of incident ion}) \tag{1.4}$$

Angle of incidence and energy of incident beam, the relative mass, surface morphology and cleanliness of target and types of bombardment influence the sputter yield directly [76].

There are three types of sputter deposition methods, which are DC (diode) Sputter Deposition, Radio frequency (RF) Sputter Deposition and Magnetron Sputter Deposition. In our experiments, we used DC Sputter Deposition Technique.

Direct Current (DC) Sputter Deposition
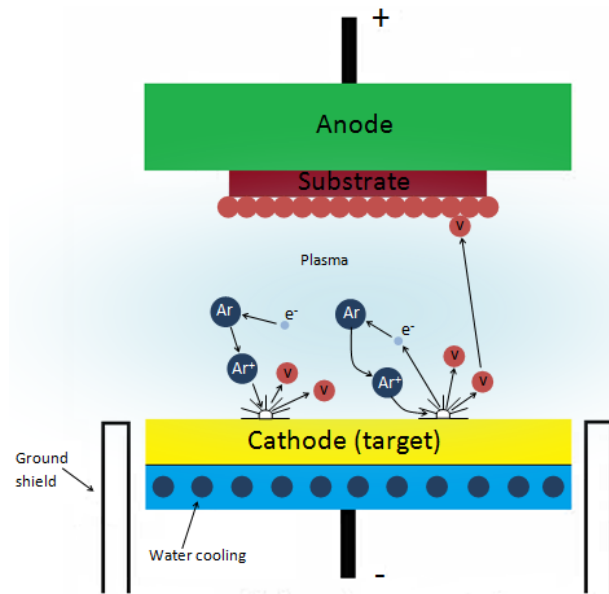
Figure 1.12. Schematic illustration of DC sputters deposition [77].

As shown in Figure 1.12, in DC sputtering process, a constant voltage (0.5-5 kV) is applied between anode (substrate) and cathode (target). An inert gas, commonly Argon, is ionized by potential difference. Ionized gaseous called plasma is the particle source, which bombards the target surface. Argon atoms enter the vacuum chamber with low pressure around 1-10 mTorr. An accelerated positive Argon ion bombards the target surface and ejects atoms from the target. Film is formed by deposition of atoms on substrate. DC Sputter can be used in electrically conductive material (cathode) because an insulator surface develops a surface charging which avoids the bombarding of the surface. The advantage of DC Sputtering is that plasma forms uniformly [78]. In our experimental procedure, substrates were settled 3.5 cm far from target. Argon gas was used for formation of plasma; and during process, the pressure of the chamber was 1.92×10^{-3} torr and substrate temperature was 500 °C.

1.2.7.3. Other Deposition Techniques

Pulsed Laser Deposition (PLD)

Also known as, laser breakout, pulsed laser deposition (PLD) was used firstly in 1987 to produce YBCO thin film [79]. Recently, PLD is continued to develop to obtain high quality film production [80]. The principle of operation of the PLD can be described briefly as follows: a pulsed laser beam, which has high energy density, focuses on the surface of the target material. Due to interaction between target and laser, surface of the target overheat and evaporate, so plasma occurs. Composed plasma contacts with heated substrate that is placed 15 cm far away from target. Thus thin film production is realized [81].

Molecular Beam Epitaxial

Molecular beam epitaxial (MBE) is the one of the vacuum evaporation techniques. In this method, thin film is deposited on substrate by molecular beam in a vacuum chamber. This process was firstly used for semiconductor thin film production. MBE can be used for film coating of a wide range of materials such as oxides and semiconductors. The composition of deposited thin film is controlled by rate of molecular beam intensity, which is controlled by temperature of molecule source. Through this process, controlling thin film thickness and the deposition of different thin films are possible. This technique achieves a layer-by-layer growth with high control. Thus, it is preferred to obtain multilayer hetero structure, which is required to have clear and sharp interfaces [82].

Chemical Vapour Deposition (CVD)

Chemical vapour deposition (CVD) is chemical reaction or decomposition of reactive gas atoms in an activated atmosphere by heat or plasma and a product formation occurs regularly. In a gas atmosphere, homogeneous gas reactions occur near the substrate. Although CVD has some disadvantages like high reaction temperature, the presence of corrosive gases and comparatively low deposition rates,

owing to production of regular, pure and reproducible thin film CVD is appealing [83].

Metal Organic Chemical Vapour Deposition (MOCVD)

Metal organic chemical vapour deposition (MOCVD), which is generally used in electronics industry, is an ideal method for the production of thin films on a large scale. In this method, metal-containing molecules are evaporated and are carried through the reactor by a carrier gas. Objective compound grows on substrate through decomposition of metal organic compounds, on substrate, by heat or composition of molecules [81]. For superconductor thin films, structure, thickness homogeneity and growth rate are controlled by heat, mass and momentum parameters [84].

PART II

EXPERIMENTAL TECHNIQUES AND RESULTS

2.1. POWDER PREPARATION

First of all, powder mixture of $Bi_2Sr_2CaCu_2O_8$ was weighted on sensitive balance which is XR 205SM-DR Precisa balance and 40g Alfa Aesar Bismuth-Strontium-Calcium-Copper-Oxide (2212) 99.9 % (metal basis) powder mixture of Bi-2212 was used for preparation of powder. Then the powder was mixed for 3 hours by using Si mortar to obtain a homogenous mixture.

2.2. $Bi_2Sr_2CaCu_2O_8$ TARGET FABRICATION

As shown in Figure 2.1, cylindrical dies consist of three parts. To create a die, Part two was placed on part one. Then obtained homogenous mixture of Bi-2212 powder was put into the part two. Finally, part three was placed into part two and cylindrical pressing die was pressed by TSEK Tümas press machine at 360 MPa for 45 minutes, shown in Figure 2.2. Thickness of the obtained cylindrical target was 0.5 cm, and diameter was 5 cm. The pressed pellet was annealed at 830 °C for 48 hours with 3 °C per minute heating and cooling rate in air by PROTHERM programmable muffle furnace. After annealing, hardness of target was of good quality, as shown in Figure 2.3. In order to place target to the DC gun, target was bonded to copper plate by Aremco-Bond silver paste. Then again, it was put in the same furnace at 180 °C for 24 hours to cement of target and copper plate. Then, the produced target was mounted on DC gun in sputtering system.
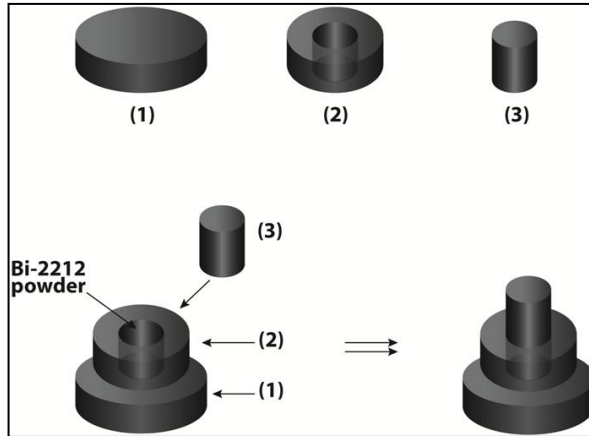
Figure 2.1. Parts of used cylindrical die.

Figure 2.2. Die in TSEK Tümas press machine.

Figure 2.3. Produced Bi-2212 target.

2.3. SUBSTRATE PREPARATION

Before coating, substrates were ultrasonically cleaned by Transsonic in deionised water, acetone and ethanol each for 15 minutes, respectively to obtain high quality thin film. After cleaning, substrates were placed into DC Sputter system.

2.4. DC SPUTTERING

$Bi_2Sr_2CaCu_2O_8$ thin films were fabricated by NSC 3000 DC Sputter Coater. Bi-2212 thin films were deposited on polished side of $SrTiO_3$ (100) substrates which were placed on a copper truncated cone (shown in Figure 2.4). Area of the truncated cone's lower base equals to area of the substrate's plate in process chamber. Thence can be reached platen temperature with minimum loss. Furthermore, it was achieved that substrates were 3 centimetres away from target (Figure 2.5 and Figure 2.6).

Figure 2.4. The substrates on copper truncated cone.
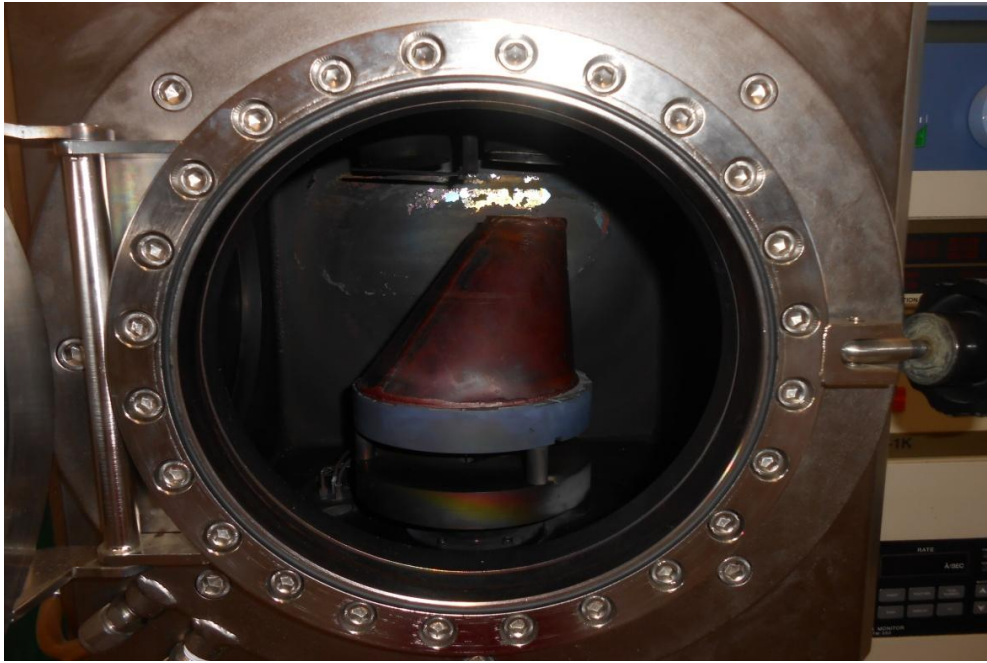
Figure 2.5. The substrates placed on copper truncated cone in sputter chamber.
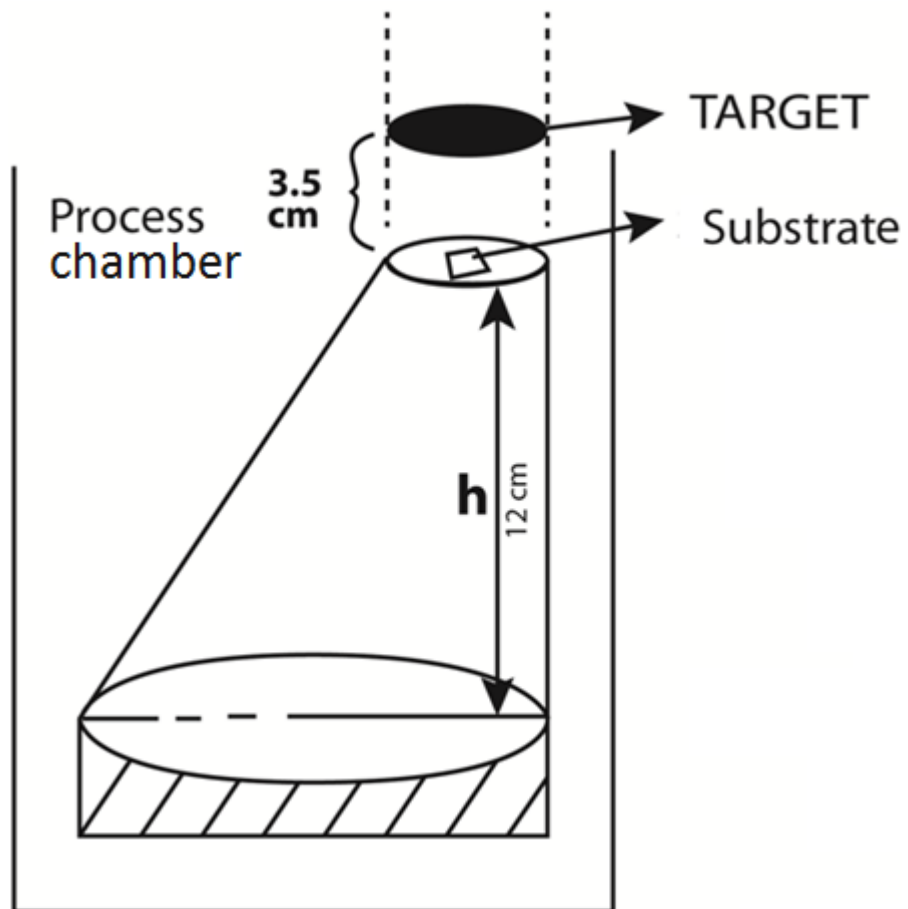
Figure 2.6. The illustration of process chamber during operation.

When vacuum process completed, the pressure of process chamber was 3.85×10^{-5} Torr. Then, Argon was sent by 20 SCCM to form the plasma and vacuum that dropped to 1.92×10^{-3} Torr. During the sputtering process, plate temperature was 500 °C and DC Power was 15 W. We produced seventeen thin films totally. Eleven of them were deposited for 2 hours and other six films were deposited for 0.5 h. Thus, we can observe the effect of deposition time on the film thicknesses. After sputtering, the surface of produced thin films was smooth and shiny as seen in Figure 2.7. Moreover, our sputter system is shown in Figure 2.8.
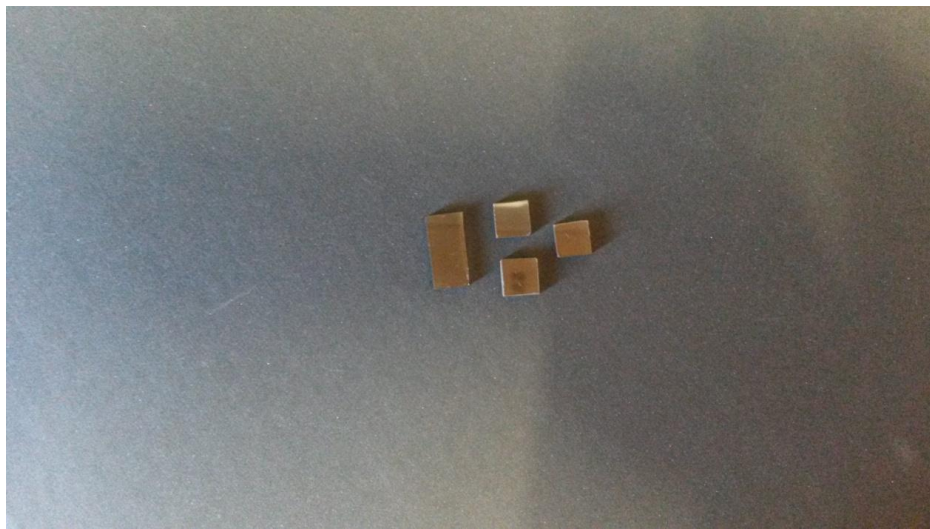
Figure 2.7. The view of substrate after sputter process.

Figure 2.8. NSC 3000 DC Sputter Coater.

2.5. ANNEALING PROCESS

Deposited thin films were annealed by using PROTHERM programmable muffle furnace shown in Figure 2.9. For all samples, the annealing time was fixed as 1h with 20 °C per minute heating and cooling rates. Figure 2.10 shows the produced thin films after annealing process. The annealing procedure of thin films was investigated using two parameters.

Figure 2.9. PROTHERM programmable muffle process.

Figure 2.10. Produced thin films after annealing process.

2.5.1. Different Annealing Temperatures

As can be seen in Table 2.1, eleven Bi-2212 thin films, which were sputtered for 2 hours, were annealed at different temperatures and all of them were in air quenched at 700 °C. After annealing process, the surface of thin films was homogenous.

Table 2.1. Parameters of E1-E11.

Designation	Deposition Time (h)	Annealing Temperature (°C)	Quenching Temperature (°C)
E1		845	
E2		850	
E3		855	
E4		856	
E5		858	
E6	2	860	700
E7		862	
E8		864	
E9		865	
E10		870	
E11		880	

2.5.2. Different Air Quenching Temperatures

Quenching is an accelerated procedure of carrying a material to room temperature. By air quenching, the material is cooled and having a chance to cause significant change in microstructure through diffusion. Air quenching has the slower cooling rate than other types of quenching. Since all these effects of quenching, we applied air quenching on thin films. Without quenching, surface of our thin films exfoliate so the topographies of thin films got worse. Owing to thin films were annealed under air atmosphere, rapid oxygen diffusion to film was provided. After quenching process, we obtained thin films that had high surface quality and we did not experience surface exfoliate problem again [85].

Other set of samples consisting of six thin films, coated for 0.5 h, which were annealed at 860°C, and air quenched at different temperatures, which are shown in Table 2.2. After annealing process, their surface, had good appearance.

Table 2.2. Parameters of E12-E17.

Designation	Deposition Time (h)	Annealing Temperature (°C)	Quenching Temperature (°C)
E12			740
E13			780
E14	0.5	860	800
E15			820
E16			840
E17			860

2.6. THICKNESS ESTIMATIONS

The mass of substrates were measured before deposition and after annealing, the density of Bi-2212 is taken as 6.6 g/cm^3, to calculate the thicknesses of produced thin films. In Table 2.3, estimations of the thicknesses of produced thin films can be seen. Due to very small change in masses, thickness calculations do not produce accurate and reliable results by this technique.

Table 2.3. Thicknesses of thin films.

Designation	Thickness (μm)	Designation	Thickness (μm)
E1	1.09	E10	0.49
E2	0.73	E11	0.52
E3	1.42	E12	0.27
E4	0.76	E13	0.49
E5	0.70	E14	0.55
E6	0.39	E15	0.42
E7	0.46	E16	0.24
E8	0.52	E17	0.79
E9	0.88		

2.7. R-T MEASUREMENTS

Resistivity versus temperature values of produced films were measured by He gas that closed cycle cryostat system (Cryo Industries). Cryostat is such a thermostat, which works at temperature below 120 K that is cryogenic temperatures. This device is supported by an external cooling source. The used coolant is usually Helium,

Nitrogen and Hydrogen, which are liquefied or solidified gas with low liquefaction and freezing temperature. Decreasing the vapour pressure over the coolant in cryostat either heating vapour of the coolant control, the temperature of a sample put in the cryostat is reduced. Cryostats have many kinds according to the type of cooling substances such as Helium, Nitrogen and Hydrogen, the type of the material used (glass, metal or plastic), function for electronic and optical and other researches such as superconducting magnets and radiation detector [86]. Our used cryostat system is shown in Figure 2.11.

The voltage and current contacts of thin films were made by the 4-probe method using high conductivity silver paint. Sample, contacted by 4-probe method and placed to cryostat can be seen in Figure 2.12 and Figure 2.13.

Figure 2.11. He gas closed cycle cryostat system (Cryo Industries).
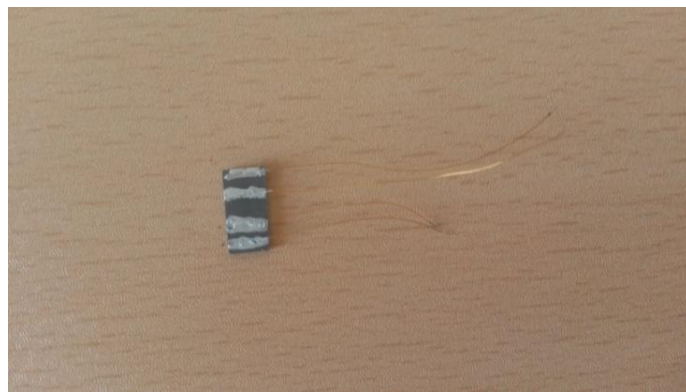
Figure 2.12. Thin film with 4-probe contacts.

Figure 2.13. Placed thin film on cryostat.

R-T measurements of the thin films for E1, E2, E3, E4, E5, E6, E7, E8, E9, E10, and E11 were taken in the temperature range of 2-150 K, which are seen in Figure 2.14 and Figure 2.15.
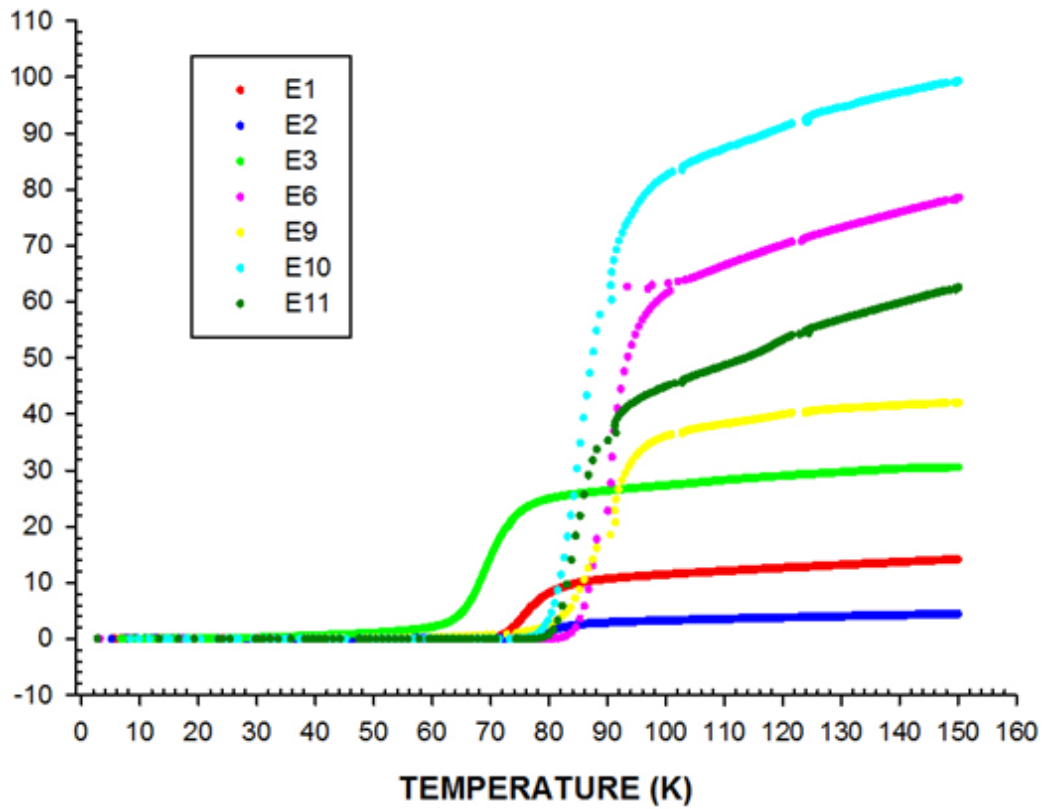
Figure 2.14. Resistivity versus temperature graph of E1, E2, E3, E6, E9, E10, E11.
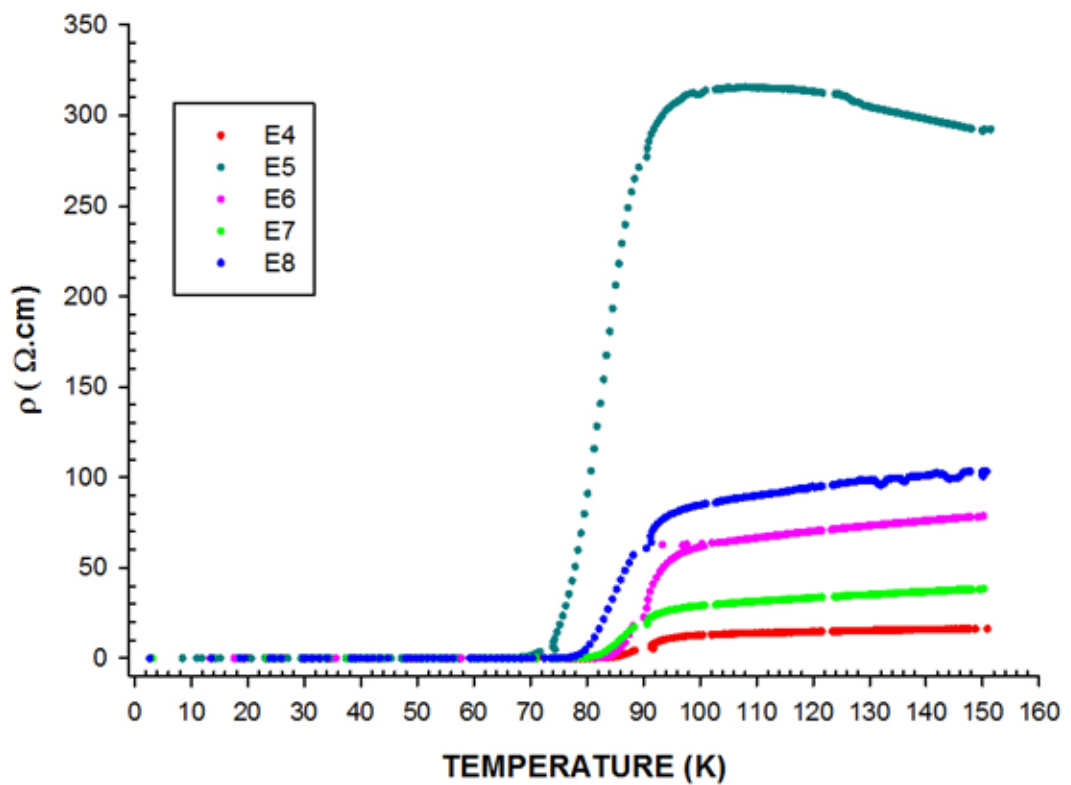
Figure 2.15. Resistivity versus temperature graph of E4, E5, E6, E7, E8.

Table 2.4. Results of R-T measurements of E1-E11.

	T_{onset} (K)	T_{offset} (K)	ΔT_c (K)	ΔR (Ohm)	R120/R150	R300K (Ohm)
E1	85	68	17	14.2041	0.8911	10.3202
E2	89	75	14	4.02375	0.849551	25.8062
E3	78	59	22	34.3091	0.9494	52.0754
E4	99	82	17	17.7477	0.89291	32.6145
E5	96	68	28	430.991	1.0735	279.4017
E6	100	82	18	44.7146	0.89407	3.7904
E7	93	75	18	37.0844	0.87177	91.1163
E8	97	74	23	115.478	0.91604	159.3841
E9	99	70	29	50.0649	0.95047	56.1767
E10	100	75	25	115.834	0.91797	154.9117
E11	92	76	16	51.51	1.1719	124.5153

The R-T values of the films, which are E12, E13, E14, E15, E16, and E17, were measured in the temperature range of 2-170K that are seen in Figure 2.16.
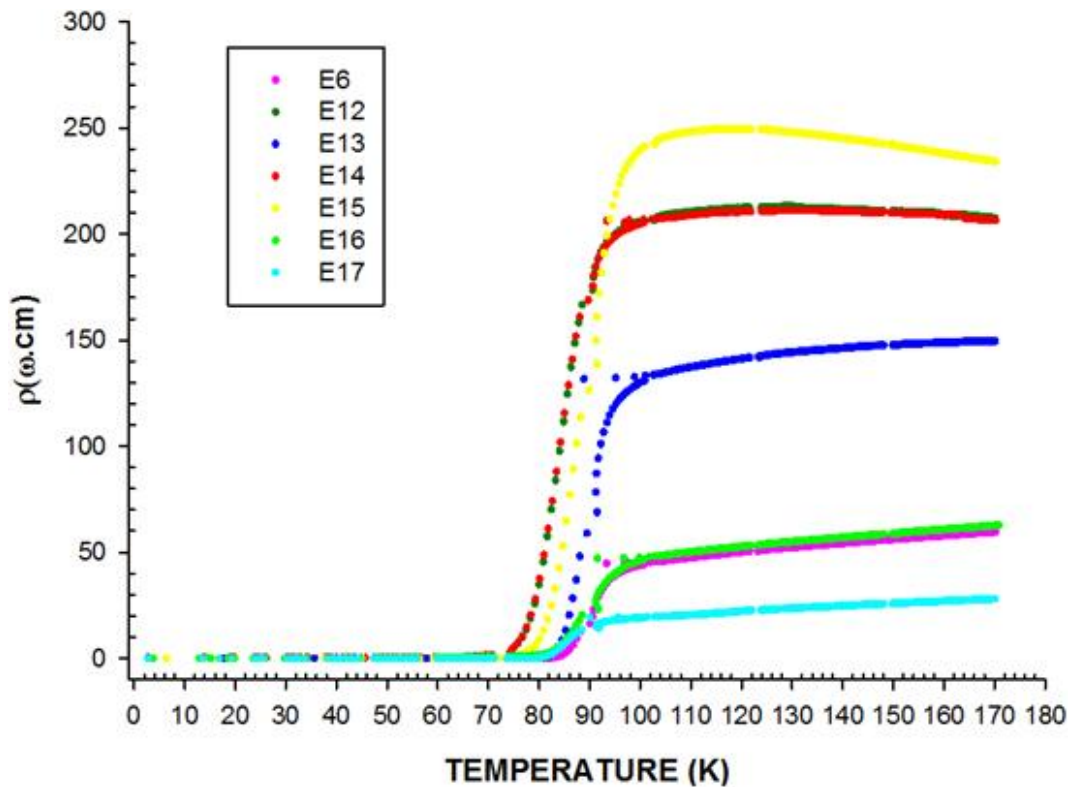
Figure 2.16. Resistivity versus temperature graph of E12- E17.

Table 2.5. Results of R-T measurements of E6 and E12-E17.

	T_{onset} (K)	T_{offset} (K)	ΔTc (K)	ΔR (Ohm)	R120/R170	R300K (Ohm)
E6	100	82	18	44.7146	0.89407	3.7904
E12	100	74	26	286.229	1.0234	239.6264
E13	100	79	21	185.888	0.945	201.1359
E14	97	68	29	283.122	1.0201	92.5508
E15	96	74	22	323.275	1.0676	120.0928
E16	100	59	41	65.3401	0.84201	116.2024
E17	100	77	23	26.7852	0.7943	53.4341

2.8. X-RAY DIFFRACTION RESULTS

X-ray diffraction provides us the answer of 'what is it'. The properties of a metal depend on the layout of atoms in crystal structure. X-ray diffraction is a non-destructive technique, which gives the fingerprint of Bragg's reflections in crystal structure [87].

2.8.1. The Operating Principle of XRD

The rays in the x-ray tube diffracts between atomic planes. Reflected rays are collected on the detector and data is obtained. The distances between the planes of atoms are achieved by angles (θ) of the peaks on the graph and Bragg equation (Eq. 2.1). Obtained distance values (d) help in predicting the current phase. Planes of atoms in different angles can be analyzed by x-ray diffraction.

$$n\lambda = 2d \sin \theta \tag{2.1}$$

where n is the integer, d is the distance between the planes of atoms and θ is the angle of incident ray with the surface plane of the sample.

If a foreign atom settles between the atoms, because of changing of distance between the planes of atoms, new formed phase can be analyzed. Obtained peaks by XRD results are compared with previous analyzing results and information about phase are

achieved. At this point, production details of analyzed material are decisive. Because, some peaks of phases can be overlapped with each other [88].

X-Ray measurements were taken by Rigaku D/Max IIIC diffractometer with CuKα. Range of measurements was $2\theta = 3°–70°$. However, we could not observe Bi-2212 phase, peaked in most of the produced thin films. We can observe Bi-2212 peaks of sample E6 that is seen in Figure 2.17 due to Sample E6 had c-axis orientation. Thus, we can say that E6 has high quality crystalline structure whose peaks were quite narrow.
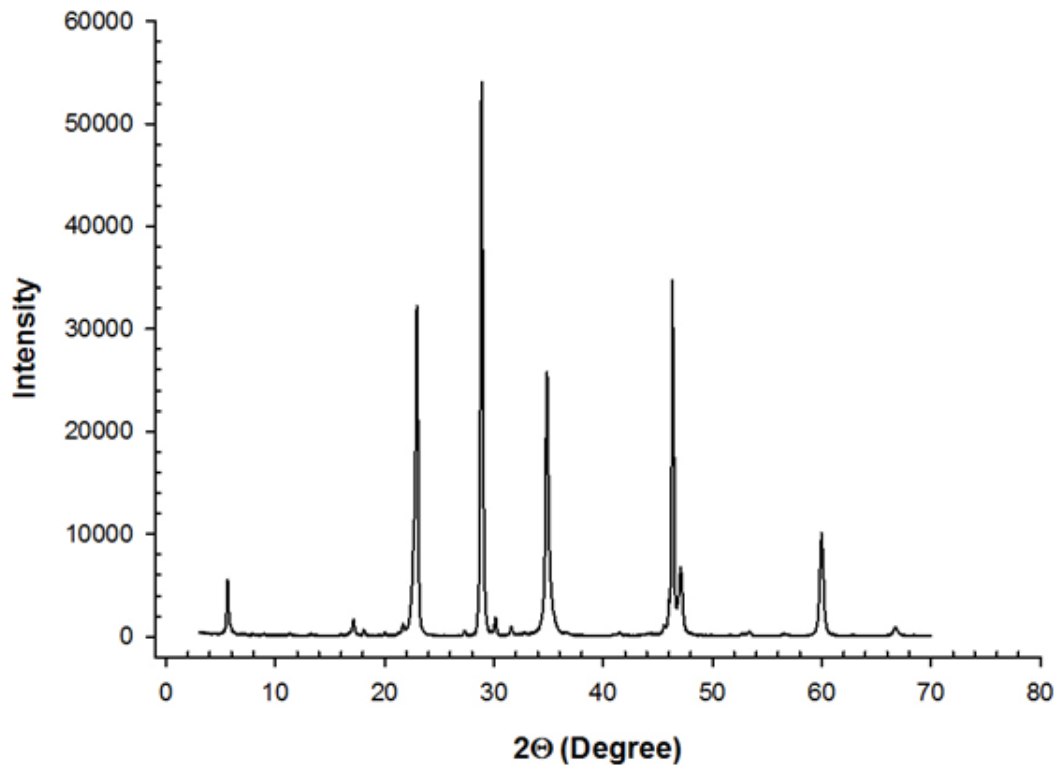
Figure 2.17. XRD pattern of E6.

2.9. SEM RESULTS

Scanning Electron Microscopy (SEM) is a useful instrument to observe unseen microscopic world. SEM is used for examining topographies of materials with a huge magnification range, which allows it to display structures of nano-scale. Classical optical microscopes use a series of glass lenses to bend light waves and form a

magnified image. SEM creates magnification of images by electron waves instead of light waves. The SEM shows quite comprehensive 3-dimensional images at much higher magnifications. Since there are no light waves, the images of SEM are black and white. The analyzed samples should be conductive to prevent vision loses due to electron accumulation, since SEM illuminates them with electrons [89].

2.9.1. How Does SEM Work?

The beam of high energy electrons are emitted by the electron gun, which is at the top of microscopy. In vacuum atmosphere, the electron beam follows a vertical path through the series of electromagnetic fields and lenses that are designed to focus the electrons to a very fine spot. As the electron beam hits the sample, electrons and x-ray are ejected from the surface of sample. The detector counts these x-rays, backscattered electrons and secondary electrons (Figure 2.18 and Figure 2.19) and convert them a signal, which is sent to an amplifier. The final image is established from the number of electrons emitted from the sample [90].
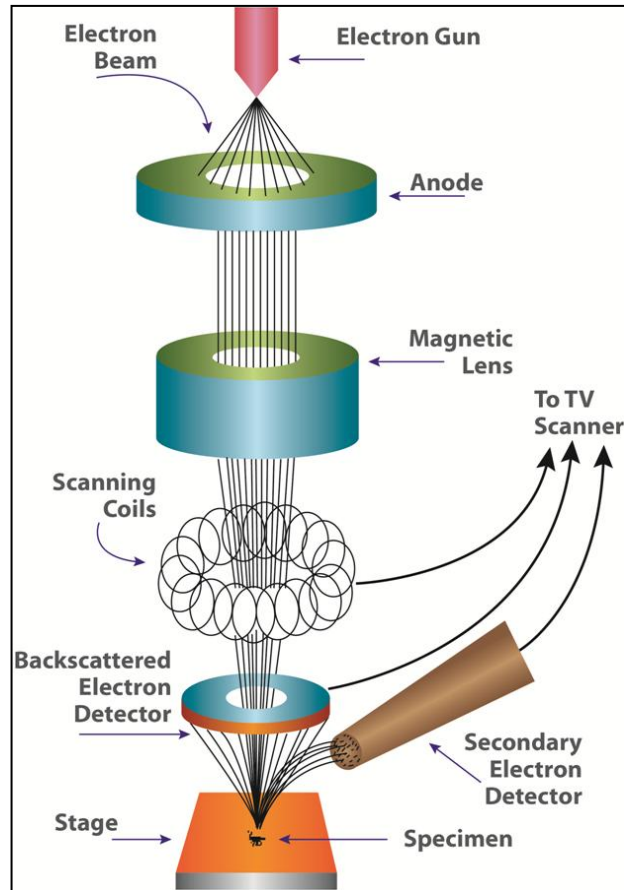
Figure 2.18. Schematic diagram of SEM [90].
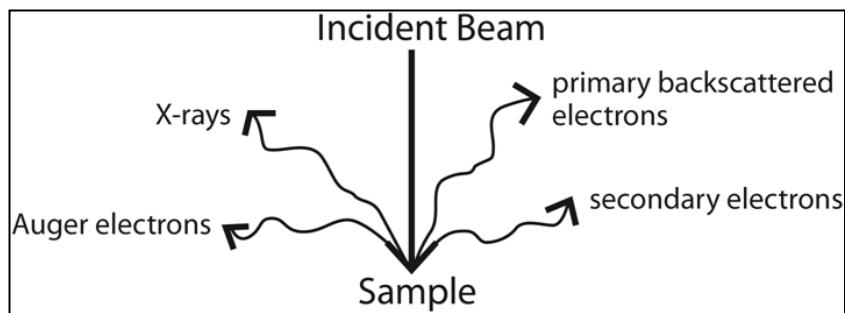
Figure 2.19. Illustration of electromagnetic waves in SEM [90].

On account of investigate the surface morphology of Bi-2212 thin film and determine the grain size and possible precipitation at the grain boundaries, samples were analyzed by SEM. Figure 2.20–Figure 2.22 show the SEM micrographs for sample E6, which was annealed at 860°C and quenched at 700°C. As can be seen, produced thin film has needle-like and flake-like grains. According to literature, these results are similar with other researcher's results.
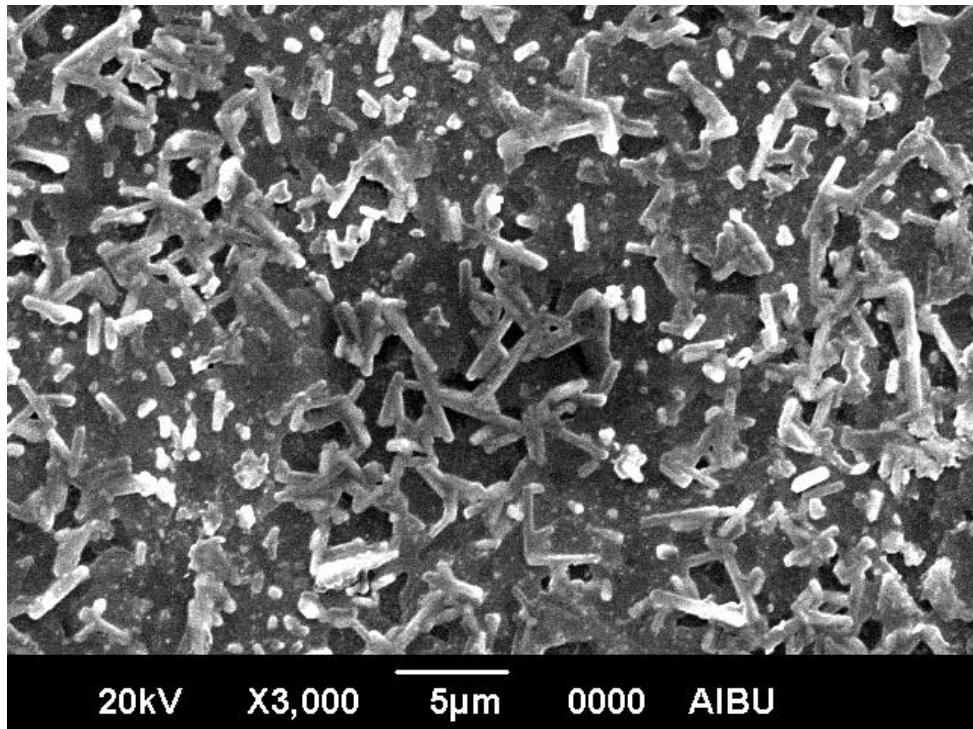
a) X3000
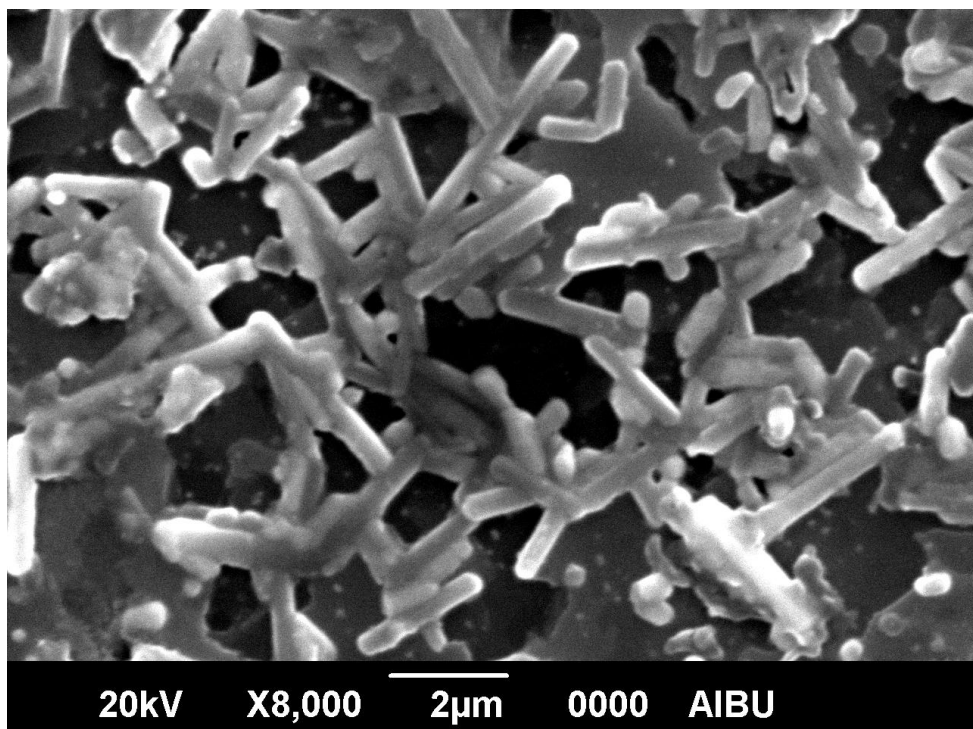
b) X8000

Figure 2.20. SEM images of E6.

20kV   X10,000   1μm   0000   AIBU
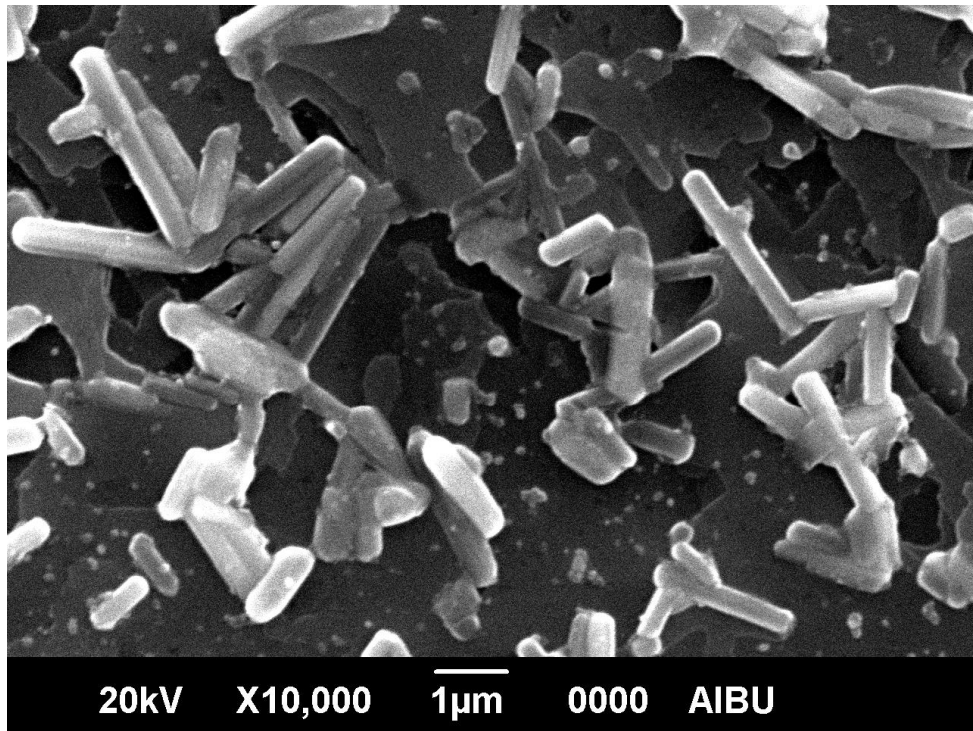
c) X10000

Figure 2.5. (continuing).

PART III

RESULTS & DISCUSSION

When we started experimental study, firstly, we used Al_2O_3 (1000) substrates. However, we could not obtain superconductive behaviour with those. We thought that the reason of these poor results was lattice mismatch between Al_2O_3 and Bi-2212. Thus, we tried to deposit film by a buffer layer, but still we could not obtain a superconductive thin film. During all these studies, we analyzed the effect of deposition time on the thickness of thin films. When DC Power value was 15 W, we deposited films for long times, such as, 6 h, 12 h, 18 h, 22 h, and 24 h. Although DC Power was right, because of long deposition time thick films were obtained instead of thin films. Furthermore, we observed that increase of platen temperature from 250 °C to 500 °C affected results as affirmative.

Owing to all of these experiences, we decided to coat thin film for 2 hours at 15 W on the $SrTiO_3$ substrates. During this process, platen temperature was 500 °C. By these parameters, we could obtain Bi-2212 superconductive thin films.

During our experiments, parameters of annealing process were investigated. We could not have enough data from literature, because, we produced thin films by ex-situ method. According to literature, thin films should be annealed at 820 °C for 1 hour with 3 °C per minute heating and cooling rate in air. We tried both increasing and decreasing heating and cooling rates, but each time, we observed surface deterioration after annealing process. The thin film, which was deposited on $SrTiO_3$ substrate for 2 hours, was annealed at 775 °C, 825 °C and 860 °C, in order, for 1 hour with 20 °C per minute heating and cooling rate and air quenched at 700 °C. After last annealing at 860 °C, we obtained a superconductive thin film. Then, we annealed another film, which was produced in the same conditions, directly at 860°C

and we again obtained affirmative results. Until that time, we experienced the annealing temperature values 845 °C, 850 °C, 855 °C, 860 °C, 865 °C, 870 °C and 880 °C. Thus, we got E1, E2, E3, E6, E9, E10 and E11 samples. Because of reaching superconductive states by annealing at 860 °C, we examined temperature close to 860 °C, such as 856 °C, 858 °C, 860 °C, 862 °C and 864 °C on samples E4, E5, E6, E7 and E8 that were annealed at above temperatures before. However, we achieved interesting results, which were not the systematic.

- In our study, optimum-annealing temperature at constant quenched temperature was 700 °C for Bi-2212 thin film and we obtained number of results showing non-linear relation of superconducting properties with annealing temperatures. That's why, we also worked on the annealing temperatures in the vicinity of 860 °C. Again, a non-linear behaviour was observed.

- According to our results, sample annealed at 860 °C and quenched at 700 °C had the maximum Tc_{offset} value with 82 K. When annealed temperature rose to 870 °C Tc_{offset} value decreased, on the other hand, room temperature resistivity increased.

- The Tc_{offset} value of sample annealed at 880 °C was little higher than sample annealed at 870 °C, but room temperature resistance value was close to the sample annealed at 860 °C and a number of Bi-2223 contribution was observed in R-T measurements. Annealed sample at the temperature of 865 °C and less than 860 °C decreased to normal state resistivity and Tc_{offset} value decreased.

- Annealed at 856 °C gave lowest normal state resistivity with high offset transition temperature. Annealing temperature of 862 °C had normal state resistivity between 860 °C and 856 °C, while its offset critical temperature slightly lower than 860 °C. 864 °C displayed higher normal state resistivity and lower critical offset temperature than the sample annealed at 860 °C.

- The most interesting one was the sample annealed at 858 °C. This sample showed semi-conductor like behaviour before transition and had very high

normal state resistivity in comparison to 860 °C and its offset critical temperature was lower. We have prepared three samples of 858 °C annealing temperature; they all showed very similar behaviour. This annealing temperature was worth further investigation.

- In accordance with all these data, optimum annealing temperature appeared to be 860 °C. For bolometer applications, a rapid change in resistivity was essential. In this respect, the sample annealed at 860 °C gave high resistivity change upon transition.

- In this thesis, we also investigated optimum quenched temperature at constant annealing temperature that was 860 °C. We observed that, when the heat treatment temperature was a direct quenched, the sample that had the lowest room temperature resistance was obtained. Moreover, the one of the observed best transition belonged to this sample.

- Although, the sample quenched at 700 °C had twice room temperature resistivity of the sample quenched at 860 °C normal state resistivity, these two samples had the similar transition temperature. Besides, the sample quenched at 840°C had the similar properties with at 860 °C and 700 °C.

- The samples quenched at intermediate temperatures, room temperature resistivity was clearly higher. When quenched temperature was fallen from 840 °C to 820 °C, the highest room temperature resistivity was obtained. Furthermore, this sample had the semi-conductive behaviour before transition.

- The samples that were quenched at 740 °C and 800 °C had the highest normal state resistivity and before transition, they showed semi-conductor like behaviour. They also had the lowest offset critical temperature. Quenched at 780 °C had the medium room temperature resistivity value.

- These results were confirmed by the measurements taken from different samples and different measurements taken from same samples. With this way, the effect of variations based on experimental conditions was minimized.

- In our thin film specimens, after 1 hour annealing time at 860 °C, cooling speed, which is until quench temperature, was kept highly proportional to temperature loss of furnace (not to be higher than 20 °C/min).

- When the sample was annealed at 860 °C for one hour, the new phase formation did not expect. The changes brought about by the different quench temperatures most likely were based on oxygen stoichiometry.

3.1. RECOMMENDATIONS

- To be a road map for researchers who want to study this discipline in future, it can be said that changing of oxygen rate of heat treatment atmosphere can modify electrical and morphological properties of thin films. Oxygen intake during cooling may probably have affected resistive behaviour of the films.

- As future work, for bolometer applications, annealing temperatures around 870 °C can be investigated. Additionally, it should be experienced that the quenched temperature should be around 700°C.

REFERENCES

1. Onnes, H. K., "Further experiments with liquid helium. D. on the change of electrical resistance of pure metals at very low temperatures, etc. V. the disappearance of the resistance of mercury", ***Koninklijke Nederlandsche Akademie van Wetenschappen Proceedings***, 14 (1): 113–115 (1911).

2. Internet: Supra Design, "Resistance, In a Superconductor: Discovery", **http://www.supraconductivite.fr/en/index.php?p=supra-resistance-supra-more** (2013).

3. Meissner, W. and Ochsenfeld, R., "Ein neuer effekt bei eintritt der Supraleitfähigkeit", ***Die Naturwissenschaften***, 21 (44): 787–788 (1933).

4. London, F. and London, H., "The electromagnetic equations of the superconductor", ***Proceedings of the Royal Society A: Mathematical, Physical and Engineering Sciences***, 149 (886): 71 (1935).

5. Ginzburg, V. L. and Landau, L. D., "On the theory of superconductivity", ***Zh. Eksp. Teor. Fiz.***, 20: 1064–1082 (1950).

6. Maxwell, E., "Isotope effect in the superconductivity of mercury", ***Phys. Rev.***, 78: 477 (1950).

7. Abrikosov, A. A., "On the magnetic properties of superconductors of the second group", ***Zh. Eksp. Teor. Fiz***, 32: 1442 (1957).

8. Bardeen, J., Cooper, L. N. and Schrieffer, J. R., "Microscopic theory of superconductivity", ***Phys. Rev.***, 106: 162–164 (1957).

9. Josephson, B. D., "Possible new effects in superconductive tunnelling", ***Physical Letters***, 1 (7): 251–253 (1962).

10. Wesche, R., "High-Temperature Superconductors: Materials, Properties and Applications", ***Kluwer Academic Publishers***, London, UK (1998).

11. Bednorz, J. G. and Muller, K. A., "Possible high T_c superconductivity in the Ba - La - Cu - O system", ***Zeitschrift für Physik B***, 64 (2): 189–193 (1986).

12. Wu, M. K., Ashburn, J. R., Torng, C. J., Hor, P. H., Meng, R. L., Gao, L., Huang, Z. J., Wang, Y. Q. and Chu, C. W., "Superconductivity at 93 K in a new mixed-phase Y - Ba - Cu - O compound system at ambient pressure", ***Physical Review Letters***, 58 (9): 908–910 (1987).

13. Michel, C., Hervieu, M., Borel, M. M., Grandin, A., Deslandes, F., Provost, J., and Raveau, B., "Superconductivity in the Bi - Sr - Cu - O system", *Zeitschrift für Physik B Condensed Matter*, 68 (4): 421–423 (1987).

14. Maeda, H., Tanaka, Y., Fukutomi, M., and Asano, T., "A new high-T_c oxide superconductor without a rare earth element", *Japanese Journal of Applied Physics*, 27 (2): L209–L210 (1988).

15. Togano, K., Kumakura, H., Maeda, H., Yanagisawa, E., and Takahashi, K., "Properties of Pb-doped Bi - Sr - Ca - Cu - O superconductors", *Applied Physics Letters*, 53 (14): 1329–1331 (1988).

16. Parkin, S. S. P., Lee, V. Y., Nazzal, A. I., Savoy, R., Huang, T. C., Gorman, G., and Beyers, R., "Model family of high-temperature superconductors: $Tl_mCa_{n-1}Ba_2Cu_nO_{2(n+1)+m}$ (m=1,2; n=1,2,3)", *Physical Review B*, 38 (10): 6531–6537 (1988).

17. Qidwai, A. A., Humayun, M., Zia-ul-Haque, S. M., Ahmad, D., and Saghir, A., "Preparation and high-T_c measurements of the $Bi_{1.6}$-Pb_x-Sb_y-Sr_2-Ca_2-Cu_3O_{delta} superconducting systems, with x=0.4, 0.3, 0.1 and y=0, 0.1, 0.3", *Superconductor Science and Technology*, 5 (10): 602–604 (1992).

18. Putilin, S. N., Antipov, E. V., Chmaissem, O., and Marezio, M., "Superconductivity at 94 K in $HgBa_2CuO_{4+\delta}$", *Nature*, 362 (6417): 226–228 (1993).

19. Chu, C. W., Gao, L., Chen, F., Huang, Z. J., Meng, R. L., and Xue, Y. Y., "Superconductivity above 150 K in $HgBa_2Ca_2Cu_3O_{8+\delta}$ at high pressures", *Nature*, 365 (6444): 323–325 (1993).

20. Nagamatsu, J., Nakagawa, N., Muranaka, T., Zenitani, Y., and Akimitsu, J., "Superconductivity at 39 K in magnesium diboride", *Nature*, 410 (6824): 63–64 (2001).

21. Kamihara, Y., Hiramatsu, H., Hirano, M., Kawamura, R., Yanagi, H., Kamiya, T., and Hosono, H., "Iron-based layered superconductor: LaOFeP", *Journal of the American Chemical Society*, 128 (31): 10012–10013 (2006).

22. Ishibashi, T., Soutome, H., Okada, Y., and Kawabe, M., "$Bi_2Sr_2Ca_{n-1}Cu_nO_y$ thin films by growth interruption technique", *Journal of Crystal Growth*, 150 (2): 1094–1097 (1995).

23. Mizuno, K. and Setsune, K., "Crystallinity for epitaxial thin films of Bi-based oxide superconductor prepared at low temperature", *Thin Solid Films*, 277 (1–2): 175–179 (1996).

24. Wiesner, J., Træholt, C., Wen, J. G., Zandbergen, H. W., Wirth, G., and Fuess, H., "High resolution electron microscopy of heavy-ion induced defects in

superconducting Bi-2212 thin films in relation to their effect on J_c", ***Physica C: Superconductivity***, 268 (1–2): 161–172 (1996).

25. Brecht, E., Linker, G., Kröner, T., Schneider, R., Geerk, J., Meyer, O., and Trlholt, C., "Growth phenomena of $Bi_2Sr_2CaCu_2O_{8+\delta}$ thin films deposited on (1 1 0) oriented $SrTiO_3$ substrates", ***Thin Solid Films***, 304 (1–2): 212–221 (1997).

26. Dreßen, J., Zakharov, N. D., Hoffschulz, H., Stahl, H., Hesse, D., and Güntherodt, G., "Preparation of BiSrCaCuO thin films by atomic layer-by-layer molecular-beam-epitaxy and high-resolution transmission electron microscopy analysis of the film/substrate interface and of growth defects", ***Journal of Alloys and Compounds***, 251 (1–2): 44–47 (1997).

27. Pfuch, A., Schmidl, F., Wiese, A., Dörrer, L., Hübner, U., and Seidel, P., "Several kinds of Josephson junctions based on BSCCO-2212 and TBCCO-2212 thin films", ***Cryogenics***, 37 (10): 685–689 (1997).

28. Haibach, P., Frey, U., Adrian, H., Lankes, F., and Renk, K. F., "Transversal thermovoltages of (1 1 9) $Bi_2Sr_2CaCu_2O_{8+\delta}$ thin films on vicinal (1 1 0) $SrTiO_3$ substrates", ***Physica C: Superconductivity***, 282–287 (2): 655–656 (1997).

29. Brecht, E., Træholt, C., Schneider, R., Geerk, J., Meyer, O., and Linker, G., "Structural properties of $Bi_2Sr_2CaCu_2O_{8+\delta}$ thin films on (1 1 0) oriented $SrTiO_3$ substrates", ***Thin Solid Films***, 319 (1–2): 215–218 (1998).

30. Rössler, R., Pedarnig, J. D., and Jooss, C., "$Bi_2Sr_2Ca_{n-1}Cu_nO_{2(n+2)+\delta}$ thin films on c-axis oriented and vicinal substrates", ***Physica C: Superconductivity***, 361 (1): 13–21 (2001).

31. Arisawa, S., Miao, H., Takano, Y., Satoh, Y., Ishii, A., Hatano, T., and Togano, K., "Growth mechanism of Bi-2212 ribbon-like thin films", ***Physica C: Superconductivity***, 362 (1–4): 301–304 (2001).

32. Kim, S. S., Moon, J. H., Lee, B. T., and Hishita, S., "Recrystallization of ion-beam amorphized $Bi_2Sr_2Ca_1Cu_2O_x$ thin films on $SrTiO_3$ (0 0 1)", ***Thin Solid Films***, 415 (1–2): 224–227 (2002).

33. Uchiyama, T., Wang, Z., and Iguchi, I., "Preparation of superconducting YBCO/Bi-2212/YBCO trilayer films for intrinsic Josephson junction devices", ***Physica C: Superconductivity***, 367 (1–4): 388–392 (2002).

34. Su, Y., Satoh, Y., Arisawa, S., Takano, Y., Ishii, A., Hatano, T., and Togano, K., "Formation processes of Bi-2212 films prepared on Ag (0 0 1) substrate by an atomization technique", ***Physica C: Superconductivity***, 372–376 (2): 619–622 (2002).

35. Endo, K., Sato, H., Yamamoto, K., Mizukoshi, T., Yoshizawa, T., Abe, K., Badica, P., Itoh, J., Kajimura, K., and Akoh, H., "Fabrication of intrinsic

Josephson junctions on BSCCO superconducting films grown by MOCVD", *Physica C: Superconductivity*, 372–376 (2): 1075–1077 (2002).

36. Kaneko, S., Shimizu, Y., Yuasa, H., and Ohya, S., "$Bi_2Sr_2Ca_1Cu_2O_X$ film prepared using 266 nm YAG laser", *Physica C: Superconductivity*, 378–381 (2): 1270–1273 (2002).

37. Kume, E., Fujino, H., Zhao, X., and Sakai, S., "Temperature dependence of composition ratio of $Bi_2Sr_2CaCu_2O_{8+\delta}$ film by PLD method", *Physica C: Superconductivity*, 412–414 (2): 1354–1357 (2004).

38. Salamati, H. and Kameli, P., "The effect of Bi-2212 phase on the weak link behavior of Bi-2223 superconductors", *Physica C: Superconductivity*, 403 (1–2): 60–66 (2004).

39. Alami, H. E. and Deville Cavellin, C., "BiSrCaCuO compounds rich in copper synthesized by molecular beam epitaxy structural and electric properties", *Journal of Crystal Growth*, 277 (1–4): 170–174 (2005).

40. Mori, Z., Doi, T., Kawabata, D., Ogata, K., Takahashi, K., Matsumoto, A., Kitaguchi, H., and Hakuraku, Y., "Growth of bi-axially textured $Bi_2Sr_2Ca_1Cu_2O_{8+\delta}$ (2 2 1 2) thin films on $SrTiO_3$ substrate by sputtering method", *Physica C: Superconductivity*, 468 (14): 1060–1063 (2008).

41. Watanabe, S., Hamanaka, K., Tachiki, T., and Uchida, T., "Investigation of in-plane orientation characteristics for Bi-2212/MgO thin films fabricated by the MOD method", *Physica C: Superconductivity*, 469 (14): 818–821 (2009).

42. Hamanaka, K., Tachiki, T., and Uchida, T., "Investigation of characteristics for different film thickness of Bi-2212/MgO fabricated by metal–organic decomposition", *Physica C: Superconductivity*, 470 (20): 1457–1460 (2010).

43. De Vero, J. C., Gabayno, J. L. F., Garcia, W. O., and Sarmago, R. V., "Growth evolution of $Bi_2Sr_2CaCu_2O_{8+\delta}$ thin films deposited by infrared (1064 nm) pulsed laser deposition", *Physica C: Superconductivity*, 470 (2): 149–154 (2010).

44. Yu, X., Yang, H., and Qi, Y., "The preparation of c-axis epitaxial Bi-2212 films on STO (1 0 0) by sol–gel method", *Applied Surface Science*, 258 (1): 38–43 (2011).

45. De Vero, J. C., Blanca, G. R. S., Vitug, J. R., Garcia, W. O., and Sarmago, R. V., "Stoichiometric transfer of material in the infrared pulsed laser deposition of yttrium doped Bi-2212 films", *Physica C: Superconductivity*, 471 (11–12): 378–383 (2011).

46. Nane, O., Özçelik, B., and Abukay, D., "The effects of the post-annealing temperature on the growth mechanism of $Bi_2Sr_2CaCu_2O_{8+\delta}$ thin films produced on MgO (1 0 0) single crystal substrates by pulsed laser deposition (PLD)", *Journal of Alloys and Compounds*, 566: 175–179 (2013).

47. Serway, R. A. and Beichner, R. J., "Chapter 27: Current and resistance", Physics for Scientists and Engineers, 5th Edition, *Brooks/Cole Pub Co*, Pacific Grove, California, US, 834 (1999).

48. İnternet: Antonine-Edu., "Resistivity", **http://www.antonineeducation.co. uk/Pages/Physics_1/Electricity/EL_04/Electricity_page_4.html** (2013).

49. İnternet: Eck, J., "Superconductivity Explained", **http://www.superconducto rs.org/oxtheory.htm** (2013).

50. İnternet: Wolfram, Inc., "Technical Data for Lead" **http://periodictable.com/ Elements/082/data.html** (2013).

51. İnternet: State of New South Wales, "Superconductors Graph", **http://lrrp ublic.cli.det.nsw.edu.au/lrrSecure/Sites/Web/physics_explorer/physics/ lo/superc_04/superc_04_01.htm** (2013).

52. Rose-Innes, A. C. and Rhoderick, E. H., "Introduction to Superconductivity", 2nd ed., *Pergamon Press*, Oxford, UK, 19–25, 31–39, 40–45, 82, 83, 118–125, 183, 184, 186–190 (1978).

53. İnternet: Oregon State University, "Chemistry 123, Latest News", **http://che mistry.oregonstate.edu/courses/ch121-3/ch123/ch123latestnews/ch123ln.htm** (2013).

54. İnternet: State of New South Wales, "Meissner Effect", **http://lrrpublic.cli. det.nsw.edu.au/lrrSecure/Sites/Web/physics_explorer/physics/lo/superc_12/s uperc_12_02.html** (2013).

55. İnternet: Hyperphysics, "Superconductivity", **http://hyperphysics.phy-astr.gs u.edu/hbase/solids/scond.html** (2013).

56. Bolonkin, A., "AB levitator and electricity storage", *Aircraft Engineering and Aerospace Technology*, 80 (4): 427–438 (2008).

57. Bulaevskii, L. N., Sobyanin, A. A. and Khomskii, D. I., "Superconducting properties of systems with local pairs", *Zh. Eksp. Teor. Fiz.*, 87: 1490-1500 (1984).

58. İnternet: Oak Ridge National Laboratory, "Type I Superconductor Graph", **http://web.ornl.gov/info/reports/m/ornlm3063r1/fig10.gif** (2013).

59. İnternet: Oak Ridge National Laboratory, "Fundamentals of Superconductors", **http://web.ornl.gov/info/reports/m/ornlm3063r1/pt3.html** (2013).

60. İnternet: Oak Ridge National Laboratory, "Type II Superconductor Graph", **http://web.ornl.gov/info/reports/m/ornlm3063r1/fig11.gif** (2013).

61. İnternet: Xabier Cid Vidal & Ramon Cid, "Superconductivity in Short", **http://www.lhc-closer.es/1/4/8/0** (2013).

62. İnternet: Robert Emery, "Ideas Implementation", **http://webs.mn.catholic.edu.au/physics/emery/hsc_ideas_implementation.htm** (2013).

63. İnternet: University of Florida, "BCS Theory and Superconductivity", **http://www.phys.ufl.edu/courses/phy4523/spring12/Sample%202.pdf** (2013).

64. Maple, M. B., "High-temperature superconductivity", *Journal of Magnetism and Magnetic Materials*, 177–181 (1): 18–30 (1998).

65. İnternet: Ankara Üniversitesi Süperiletken Teknolojileri Uygulama ve Araştırma Merkezi, "Bi-Tabanlı Süperiletkenler", **http://cesur.ankara.edu.tr/superiletke nlik-hakkinda/superiletken-malzemeler/yuksek-sicaklik-superiletken-hts-malzemeler/bi-tabanli-superiletkenler/** (2013).

66. Tarascon, J. M., LePage, Y., Greene, L. H., Bagley, B. G., Barboux, P., Hwang, D. M., Hull, G. W., McKinnon, W. R. and Giroud, M., "Origin of the 110-K superconducting transition in the Bi - Sr - Ca - Cu - O system", *Physical Review B*, 38 (4): 2504–2508 (1988).

67. Türkoğlu, S., "Ultrasonik sprey piroliz (USP) yöntemi ile $Bi_2Sr_2Ca_2Cu_3O_{10+\gamma}$ süperiletken filmlerin hazirlanmasi ve karakterizasyonu", Yüksek Lisans Tezi, *İnönü Üniversitesi Fen Bilimleri Enstitüsü*, 17, 18 (2011).

68. Phillips, J. M., "Substrate selection for high-temperature superconducting thin films", *Journal of Applied Physics*, 79 (4): 1829–1848 (1996).

69. Sato, H., Naito, M., Tsukada, A., Karimoto, S., and Matsuda, A., "Influence of substrates on epitaxial thin films of high-temperature superconductors", *Physica C: Superconductivity*, 362 (1–4): 186–194 (2001).

70. İnternet: University of Florida, "Semiconductor Laboratory Course Manual", **http://www.che.ufl.edu/ren/course/Semicond%20Lab/manual/sputtering/N T.pdf** (2013).

71. Behrisch, R., Roth, J., Staudenmaier, G. and Verbeek, H., "Sputtering in fusion devices", *Nuclear Instruments and Methods in Physics Research Section B: Beam Interactions with Materials and Atoms*, 18 (1–6): 629–638 (1986).

72. Ziegler, J. F., "The Stopping and Range of Ions in Solids, 2nd Ed.", *Academic Press*, Waltham, Massachusetts, US, 3-61 (1988).

73. Sckerl, M. W., Vicanek, M., and Sigmund, P., "Momentum in atomic collision cascades", *Nuclear Instruments and Methods in Physics Research Section B: Beam Interactions with Materials and Atoms*, 102 (1–4): 86–92 (1995).

74. Thompson, M. W., "Physical mechanisms of sputtering", *Physics Reports*, 69 (4): 335–371 (1981).

75. Behrisch, R. and Eckstein, W., "Sputtering yield increase with target temperature for Ag", *Nuclear Instruments and Methods in Physics Research Section B: Beam Interactions with Materials and Atoms*, 82 (2): 255–258 (1993).

76. İnternet: Kobelco Research Institute, "The Sputtering Target Division", **http://www.kobelcokaken.co.jp/target/english/index.html** (2013).

77. İnternet: Micro Magnetics, Inc., "Magnetron Sputtering Technology", **http://www.direct vacuum.com/sputter.asp** (2013).

78. Depla, D., Mahieu, S., and Greene, J. E., "Chapter 5 - Sputter deposition processes", Handbook of Deposition Technologies for Films and Coatings, 3rd Edition, *William Andrew Publishing*, Boston, US, 253–296 (2010).

79. Krebs, H. U., Weisheit, M., Faupel, J., Süske, E., Scharf, T., Fuhse, C., Störmer, M., Sturm, K., Seibt, M., Kijewski, H., Nelke, D., Panchenko, E., and Buback, M., "Pulsed Laser Deposition (PLD) – A versatile thin film technique", Advances in Solid State Physics, *Springer*, Berlin, Heidelberg, Germany, 505–518 (2003).

80. Singh, R. K. and Kumar, D., "Pulsed laser deposition and characterization of high-T_c YBa$_2$Cu$_3$O$_{7-x}$ superconducting thin films", *Materials Science and Engineering: R: Reports*, 22 (4): 113–185 (1998).

81. Soltan, S. E. A. G., "Interaction of superconductivity and ferromagnetism in YBCO/LCMO heterostructures", Ph. D. Thesis, *Max-Planck-Institut Für Festkörperforschung der Universität Stuttgart*, Stuttgart, Germany, 59–61 (2005).

82. Odier, P., Supardi, Z., De-Barros, D., Vergnières, L., Ramirez-Castellanos, J., Gonzales-Calbet, J. M., Vallet-Regi, M., Villard, C., Peroz, C., and Weiss, F., "Spray pyrolis for high T_c superconductors films", *Superconductor Science and Technology*, 17 (11): 1303 (2004).

83. Hakuraku, Y., Koba, S., Higo, S., Nakao, A., and Ogushi, T., "Ultrathin film preparation of superconducting 2223 Bi(Pb)SrCaCuO by sputter deposition and rapid annealing", *Superconductor Science and Technology*, 9 (1): 23 (1996).

84. Xiong, J., Qin, W., Cui, X., Tao, B., Tang, J., and Li, Y., "Thickness-induced residual stresses in textured YBCO thin films determined by crystalline group method", *Physica C: Superconductivity*, 455 (1–2): 52–57 (2007).

85. İnternet: About.com, "Quenching", **http://metals.about.com/od/metallurgy/g/Quenching.htm** (2013).

86. İnternet: Farlex, Inc., "Cryostat", **http://encyclopedia2.thefreedictionary.com /Cryostat** (2013).

87. İnternet: The University of Sheffield, "The X-ray Diffraction Small Research Facility: What is XRD?", **http://www.sheffield.ac.uk/materials/research/cen tres/2.4449/whatxrd** (2013).

88. İnternet: Moeck, P., "X-ray Diffraction (XRD)", **http://web.pdx.edu/~pmoeck/ phy381/Topic5a-XRD.pdf** (2013).

89. İnternet: Swapp, S., "Scanning Electron Microscopy (SEM)", **http://serc.carl eton.edu/research_education/geochemsheets/techniques/SEM.html** (2013).

90. İnternet: Schweitzer, J., "Scanning Electron Microscope", **http://www.purdue. edu/rem/rs/sem.htm** (2013).

RESUME

Esra EVCİN BAYDİLLİ was born in İzmir and she graduated first and elementary education in this city. She completed high school education in İzmir Bornova Anatolian High School, after that, she started undergraduate program in Abant İzzet Baysal University Department of Physics in 2004. Then in 2012, she started assignment as a Research Assistant in Hakkari University Department of Electrical and Electronics Engineering. To complete M. Sc. education, she moved to Karabük University, where she has been still working as a R. A. for.

CONTACT INFORMATION

Address: Karabük University

Graduate School of Natural & Applied Science

Demir-Çelik Campus/KARABUK

E-mail: esraevcin@karabuk.edu.tr; esraevcin@gmail.com